

A Classification Atlas of Stellar Spectra of Luminosity
Types III and V for the Burke - Gaffney Observatory

by

Robert G. Bailey

A Dissertation Submitted to the Faculty of the

Department of Astronomy

In partial fulfillment of the requirements
for the degree of

Master of Science

Saint Mary's University

© Copyright

1978

TABLE OF CONTENTS

	Page
LIST OF TABLES	v
LIST OF ILLUSTRATIONS	vi
ABSTRACT	viii
I. INTRODUCTION	1
II. SPOTZ SPECTROGRAPH	3
i) Grating	3
ii) Collimator	3
iii) Camera	3
iv) Filter	4
v) Decker	4
vi) Slit Width Dial Calibration	6
III. SPECTROGRAPH TESTING AND PREPARATIONS	8
i) Focusing Test Plates	8
ii) Comparison Line Identification	12
iii) Reciprocal Dispersion	15
iv) Adopted Camera Focus Settings	17
IV. PRODUCTION OF STELLAR SPECTROGRAMS	18
i) Spectrograph Operating Settings	18
ii) Spectrograph Operating Procedure	23
iii) Exposure Curve Recalibration	24

TABLE OF CONTENTS Continued

	Page
V. PRODUCTION OF AN MK CLASSIFICATION ATLAS	29
i) Selection of Program Stars	29
ii) Darkroom Processing	29
iii) MK Atlas	30
iv) Atlas Plates 1 and 2	31
v) Classification of Unknown Spectra	37
vi) Classification of Unknown Program Stars.	38
VI. VARO IMAGE TUBE CAMERA	41
i) Description	41
ii) Power Supply	41
iii) General Manufacturer's Specifications ..	41
VII. IMAGE TUBE TESTING	44
i) Image Tube Operating Settings	44
ii) Reciprocal Dispersion	45
VIII. PRODUCTION OF IMAGE TUBE SPECTROGRAMS	48
i) Introduction	48
ii) Image Tube Exposure Times	48
iii) Image Tube Classification of Program Stars	50
IX. SPECTRUM OF THE NIGHT SKY AT HALIFAX	62
i) Blue-Violet Region (3900 - 4700 Å)	62
ii) Red Region (4700 - 6000 Å)	62

TABLE OF CONTENTS Continued

	Page
X. THESIS RESULTS AND RECOMMENDATIONS	66
APPENDIX A COMPARISON LINE IDENTIFICATION AND HARTMAN CURVE CONSTRUCTION - CLASSICAL	
CAMERA	A1
i) Blue-Violet Region ($\lambda < 4600 \text{ \AA}$)	A1
ii) Red Region ($\lambda > 5000 \text{ \AA}$)	A4
BIBLIOGRAPHY	A7

LIST OF TABLES

Table		Page
1.	Decker Positions and Patterns	5
2.	Spectrograph Operating Settings (Grating BL280).	10
3.	Exposure Curve Recalibration	27
4.	Atlas Sequence of V Stars (Plate 1)	33
5.	Atlas Sequence of III Stars (Plate 2)	34
6.	Image Tube Exposure Times	51
7.	Classification of Program Stars	59
A1.	Data for the Comparison Line Identifications and Hartman curve construction for the Blue-Violet Region	A2
A2.	Data for the Comparison Line Identifications and Hartman Curve Construction for the Red Region	A5

LIST OF ILLUSTRATIONS

Figure		Page
1.	Calibration of the Spectrograph Slit Dial	7
2.	Adopted Comparison Line Identifications for the Blue-Violet Region	14
3.	Adopted Comparison Line Identifications for the Red Region	16
4.	Exposure versus Apparent Magnitude Relation for the Classical Spectrograph	21
5.	Exposure versus Apparent Magnitude Relation for the Classical Spectrograph using the Neutral Density Filter	22
6.	Recalibration Factor versus Apparent Magnitude (m_B)	28
7.	Photocathode Spectral Response Curve of the Varo Image Tube	43
8.	Exposure versus Apparent Magnitude Relation with the Varo Image Tube	52
9.	Blue-Violet Region of the Night Sky Spectrum	64
10.	Red Region of the Night Sky Spectrum	65
11.	Hartman Curve for the Blue-Violet Region	A3
12.	Hartman Curve for the Red Region	A6

PLATES

Plate		Page
1.	B.G.O. Atlas - Main Sequence Spectrograms	35
2.	B.G.O. Atlas - Giant Spectrograms	36
3a.	Classical and Image Tube Spectrograms of the	60
3b.	Program Stars	61

A Classification Atlas of Stellar Spectra of Luminosity
Types III and V for the Burke - Gaffney Observatory

by Robert G. Bailey

Date of Submission 24 Aug. 1978

Abstract

The MK classification system is defined by the spectra of an array of standard stars and is based on the appearances and relative intensities of selected spectral lines, blends, and bands observed in the blue-violet region of the spectrum. In spite of recent studies showing the necessity of revising the system to include an abundance parameter, the MK system remains a two dimensional classification system based on temperature types and luminosity classes.

A Spitz spectrograph which was recently acquired by the Burke - Gaffney Observatory, was used after an initial period of testing, to produce a series of spectrograms of selected MK standard stars of luminosity types III and V. The testing period was necessary to obtain the correct spectrograph operating settings (camera focus, grating tilt, slit width, and stellar exposure times) and to devise a satisfactory observing procedure for photographing stellar spectra in the blue-violet wavelength region. The resulting photographic sequence or atlas of spectrograms could then be used at the Burke - Gaffney Observatory to assign MK classifications to other stars. Eleven program stars were employed to test the classification capability and accuracy of the

produced atlas. The results proved very satisfactory as in all cases the atlas - assigned spectral types were within one subclass of the accepted classifications and nine of the eleven stars were given the correct luminosity classes.

Secondary objectives involved the testing of the classification capacity of the spectrograph when using the Observatory's Varo image tube and a study of the Halifax night sky spectrum. The results of the image tube testing indicated that a classification atlas using this apparatus may prove valuable and should be produced. The night sky spectrum of Halifax was heavily marked with emission lines from mercury and sodium vapour lamps.

INTRODUCTION

Before any new instrument can be properly used for research, it is essential that it be examined, checked, and carefully tested under various conditions. This period of testing is necessary to obtain a complete understanding of the correct operating procedure and the limitations of the apparatus. In many cases, the instrument must be calibrated and checked by attempting to quantitatively reproduce known results, or by qualitative comparison with accepted standards. In the case of a spectrograph to be used for stellar classification, the initial testing and final calibration stages naturally lead to a comparison of the spectrograms produced to those of an atlas of stellar spectra based on a standard classification system.

The MK classification system in a brief outline may be described as follows:-

- 1) It is a spectral classification system based on the appearances and relative intensities of selected spectral lines, bands, and blends observed in the visual region of the spectrum.

- 2) The system is defined by the spectra of an array of standard stars.

3) In spite of recent studies showing the necessity of revising the system to include an abundance parameter, the MK system remains a two dimensional classification system based on temperature types and luminosity classes.

The objectives of this thesis are to test the newly - acquired Spitz spectrograph of the Burke - Gaffney Observatory, to obtain the necessary operating calibrations (camera focus, grating tilt, slit width, and exposure times), to identify the wavelengths of lines in the comparison spectrum, and to devise a satisfactory observing procedure for photographing stellar spectra in the blue-violet region. With this information, the spectrograph is then used to produce a series of spectrograms of selected MK standard stars of the giant and main sequence luminosity classes. Careful examination of these photographs is necessary to see whether the important MK classification features are visible. The resulting photographic sequence can then be employed to assign classifications to other stars. Secondary objectives are to study the spectrum of the Halifax night sky and to test the classification capacity of the spectrograph when using the Observatory's Varo image tube.

II

SPOTZ SPECTROGRAPH

The specifications of the spectrograph are as follows:-

i) Grating:-

Bausch and Lomb plane reflection grating

Catalogue Number - 35-53-06-280
(or B.L 280)

Serial Number - 2653-57-15-2

Grating Size - 57.2mm X 57.2mm.

Blazed at 5000 Å in the first order

Nominal Reciprocal Dispersion 80 Å/m.m.

1200 Grooves per m.m.

ii) Collimator:-

Jaegers Coated Achromat

Diameter - 42.0 m.m.

Focal Length - 277.0 m.m.

iii) Camera:-

Focal Length - 101.6 m.m.

f/4

Demagnification factor = $\frac{277.0}{101.6} = 2.73$

iv) Filter:-

The shutter slide position #1 was fitted with a neutral density filter to permit observing stars brighter than $m_B = 3.0$. This slide position is the first shutter detent location obtained by pulling the shutter knob outward from the closed position. The second slide position with the shutter knob pulled completely outward has no filter and admits all the light passing through the slit into the spectrograph.

The neutral density filter is:-

Baird Atomic Filter

Catalogue Number 110-0889-04









Density 0.90

A density of 0.90 corresponds to a stellar magnitude increase of $2^m.25$.

v) Decker:-

The decker of the spectrograph controls the pattern of light which enters the instrument and falls upon the photographic plate. The decker positions and patterns are shown in Table 1. Both the actual decker slit and projected plate dimensions were measured with a Gaertner measuring engine. The measured plate dimensions show very good agreement to those calculated values obtained using the decker slit dimensions and the 2.73 demagnification factor.

Table 1 Decker Positions and Patterns

Decker Position	Slit Pattern	Actual Slit Dimension (in m.m.)	Projected Dimension on Plate (in m.m.)	Comments
1.	Full Slit	-	-	
2.	 a  b	a = 1.21 b = 1.56	a = 0.44 b = 0.56	Narrow comparison spectrum Matches position 3 for object
3.	 a	a = 1.20	b = 0.40	Narrow stellar spectrum Projected Slit Length = 54
4.	 a  b  a	a = 1.19 b = 2.77	a = 0.44 b = 0.99	Wide comparison spectrum Matches position 5 for object.
5.	 a	a = 2.32	a = 0.84	Wide stellar spectrum. Projected slit length = 104
6.	 a	a = 4.07	-	Projected slit length = 183 Use without comparison spectrum or when overlapping comparison can be tolerated
7.	Closed Slit	-	-	Slit Covered.

vi) Slit Width Dial Calibration:-

Calibration measurements of the slit width dial were made with the Gaertner measuring engine. Figure 1, showing the slit width versus dial setting, was constructed from these measured values. The measured widths were converted into units of seconds of arc using the following relationship:-

$$\begin{array}{l} \text{Projected Slit Width} \\ \text{(in sec. of arc)} \end{array} = \begin{array}{l} \text{(linear slit width)} \\ \text{(in sec. of arc)} \end{array} \times \begin{array}{l} \text{(telescope} \\ \text{scale)} \end{array}$$

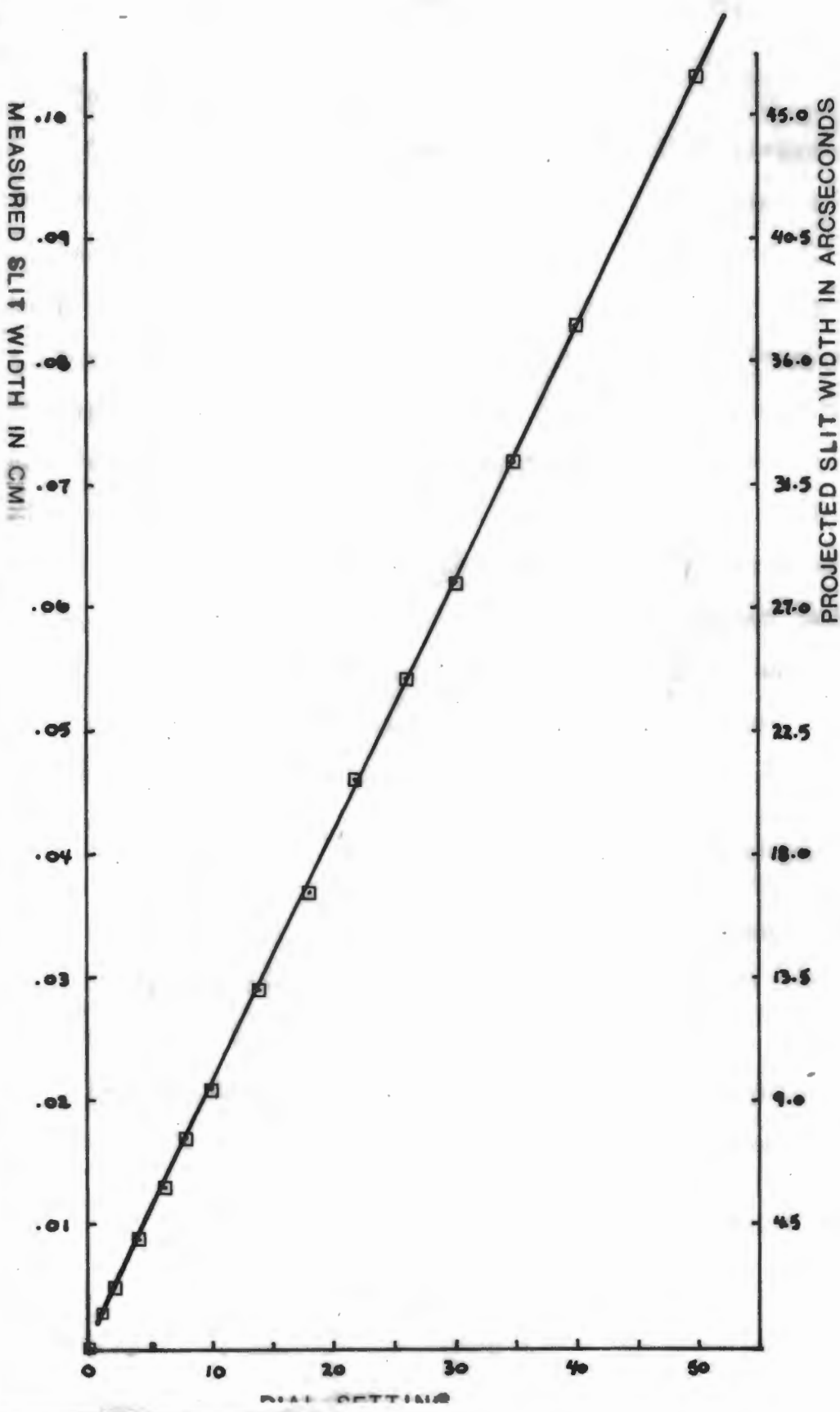
with the telescope scale = $45''$ per m.m.

Figure 1

Calibration of the Spectrograph slit dial

The straight line is fitted by eye to the measurements.

SLIT DIAL SETTING	WIDTH IN CM.
0	0
1	0.003
2	0.005
4	0.009
6	0.013
8	0.017
10	0.021
14	0.029
18	0.037
22	0.046
26	0.054
30	0.062
35	0.072
40	0.083
50(0)	0.103



III

SPECTROGRAPH TESTING AND PREPARATIONS

i) Focusing Test Plates

The initial step of spectrograph testing involved using the comparison lamp to obtain the best combination of comparison spectrum exposure time, camera focus, and slit width to produce sharp comparison lines; and to find the grating tilt setting which centers various spectral regions on the photographic plate. Initially the comparison spectrum was observed directly through the plateholder - camera opening with a magnifying lens. This procedure provided an initial grating tilt, slit width, and a rough camera focus setting. Using this information, test plates with selected ranges of exposure times, focus settings, and slit widths were taken. With each successive plate, the trial range of settings was narrowed. The results are given below.

a) Blue - Violet Region ($\lambda < 4600 \text{ \AA}$)

Among the 23 lines observed in this half of the comparison spectrum, a very close doublet was found centrally located. By using this doublet as a focus indicator, a best focus of 2.98 was selected. This doublet was later identified as Ar lines of wavelengths 4198.32 \AA and 4200.68 \AA . Various trial slit widths

were selected. It was found that slit widths greater than 1.5 did not clearly resolve the Ar doublet. Based on this observation, a slit width of 1.5 was adopted for testing purposes. It was noted, however, that this slit width, which corresponds to $1.8''$, is somewhat wide for stellar work. A grating tilt setting of 1.10 was found to centrally position the blue-violet lines on the plate and an exposure time of 10 seconds was selected.

b) Red Region ($\lambda > 5000 \text{ \AA}$)

A number of faint and reasonably close doublets within this region were used as focus indicators. A best focus of 2.74 was selected. The slit width dial setting was fixed at 1.5. The exposure time was found to be within the range of 20 to 30 seconds.

The grating tilt setting for this region is described as the "inner stops". In order to centrally locate the comparison lines of this region on the plate, it was necessary to turn the grating tilt micrometer inward beyond the dial zero position as far as the micrometer would allow. (ie. approximately two complete turns inward past the zero position)

Table 2 lists the spectrograph settings for the two regions as adopted from the test plates. It was noted that the camera focus settings were not only different for the two halves of the comparison spectrum but also varied noticeably with wavelength within each region. The focus settings shown in Table 2 are those which gave the best focus for the centrally positioned lines of each region (4200 Å for the blue-violet region and 5800 Å for the red region.)

Table 2 Spectrograph Settings

(Grating B.L. 280)

	Blue Violet Region ($\lambda < 4600 \text{ \AA}$)	Red Region ($\lambda > 5000 \text{ \AA}$)
Camera Focus	2.98 (For 4200 \AA)	2.74 (For 5800 \AA)
Exposure Time	10 seconds	20-30 seconds
Grating Tilt	1.10	"inner stops"
Slit Width	1.5	1.5

ii) Comparison Line Identification

Only after identification of the comparison lines has been made can an accurate list of best focus settings versus wavelength be produced. The comparison lines which are used to provide the identification and wavelength of the stellar spectral lines were identified by the following method.

1. The composition of the gas within the lamp producing the comparison lines provided a starting point for line identification. The comparison spectrum of the Spetz spectrograph was produced by a neon lamp.¹ Except for the neon, the composition of the gas within the bulb was not known; however, based on considerations of chemistry, it was assumed that the neon would be contaminated by the other noble gases.

2. The appearances, relative intensities, and rough estimates of the line wavelengths were then compared to the standard reference list of spectral lines as given in the Handbook of Chemistry and Physics.

3. To confirm the tentative identifications of the comparison lines, a Hartmann Correction curve was constructed. (see Appendix A)

4. This identification procedure was applied separately to the blue-violet and red regions of the comparison spectrum.

1. Bulb manufactured by Canadian Miniature Lamps.
Bulb type NE 30, 1 watt, 105 - 125 volts.

a) Blue-Violet Region ($\lambda < 4600 \text{ \AA}$)

Figure 2 shows the adopted identifications of the comparison lines in the blue-violet region of the spectrum. These lines were identified by measuring spectrum # 12 of focus test plate C.T # 7¹ with the Gaertner measuring engine. With the measured positions of the lines and the lab wavelengths of the spectral lines of the noble gas as given in the Handbook of Physics and Chemistry, the comparison lines were assigned tentative identifications. To confirm these identifications, a Hartman curve (Figure A1) was constructed. Appendix A lists the measured line positions, the calculated Hartman wavelengths (λ_H) and the resulting wavelength residuals ($\Delta\lambda$). The resulting Hartman curve (Figure A 1) is also shown.

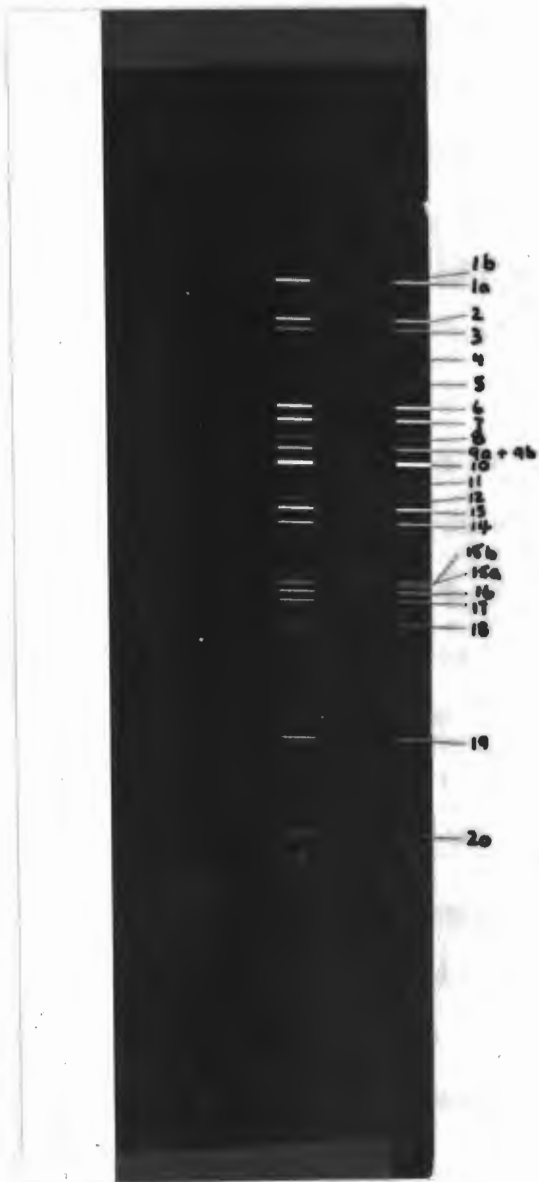
Based on the low $\Delta\lambda$ values, and the smooth shape of the Hartman curve, the preliminary line identifications were confirmed. All ($|\Delta\lambda|$) values were found to be less than 0.30 \AA with the exceptions of line 7 ($\Delta\lambda = + 0.56$) and line 11 ($\Delta\lambda = - 0.57$). For these two lines measuring errors may have produced the large $\Delta\lambda$ values, or the lines may have been misidentified, or perhaps are blends. Line 4 was found to be faint and too irregular in shape to be accurately measured with the Gaertner engine and hence a Hartmann wavelength was not calculated.

1. C.T # 7 represents the plate number as entered in the BGO Spectrograph Logbook. The letters C.T indicate a classical test plate using the comparison lamp.

Figure 2

The adopted line identifications for the blue-violet region ($\lambda < 4600 \text{ \AA}$) of the comparison spectrum (using grating BL 280)

Fig 2, KIT



REF #	SOURCE	λ_{lab}
1b	Ar	4510.73
1a	Kr	4502.36
2	Kr	4463.69
3	Kr	4453.92
4		
5	Kr	4399.97
6	Kr	4376.12
7	Nb	4363.52
8	Ar	4345.17
9b	Ar	4335.34
9a	Ar	4333.56
10	Kr	4319.58
11	Ar	4300.10
12	Kr	4282.97
13	Kr	4273.97
14	Ar	4259.36
15b	Ar	4200.68
15a	Ar	4198.32
16	Ar	4191.03
17	Ar	4181.88
18	Ar	4158.59
19	Ar	4044.42
20	Ar	3948.98

b) Red Region ($\lambda > 5000 \text{ \AA}$)

Figure 3 lists the identified lines in the red region of the comparison spectrum. These lines were identified from spectrum 9 of focus test plate C.T #6. The identifications were confirmed with the construction of a Hartman curve (Figure A.2). Appendix A contains all the necessary information required in the production of this curve.

All the identified lines possess $|\Delta\lambda|$ values less than 0.50 \AA except for line 5 ($\Delta\lambda = -0.62$) and line 7 ($\Delta\lambda = +0.58$). For these two lines, measuring errors, line misidentification, or line blending may explain the large values. As the plotted point for line 7 falls well of the general trend of the Hartman curve, it is believed that this line has been misidentified. Lines 1, 2, 8, 10, 12, and 18 were too faint to be accurately measured and could not be identified. The positions and relative intensities of lines 1 and 2 do, however, appear to match the Ne lines at 5330.78 \AA and 5341.09 \AA respectively. The two identifications should be regarded as tentative. Lines 6, 14, 23, 25, and 27, which are all thin and faint in appearance, could not be matched to any noble gas or iron spectral lines.

iii) Reciprocal Dispersion

Using the identified wavelengths of the comparison lines and their measured positions, the reciprocal dispersion (D) of the comparison spectrum was calculated as:-

$$D = \frac{\Delta\lambda}{\Delta x}$$

Figure 3

The adopted identifications of the comparison lines in the red region of the spectrum ($\lambda > 5000 \text{ \AA}$) (using grating BL 280).

Fig 3, P16



Ref. #	Source	λ_{lab}
9	Ne	5764.42
10	-	-
11	Ne	5820.15
12	-	-
13	Ne	5852.49
14	-	-
15	Kr	5870.92
16	Ne	5881.90
17	Ne	5902.46
18	-	-
19	Ne	5944.83
20	Ne	5965.47
21	Ne	5975.53
22	Ne	5987.91
23	-	-
24	Ne	6029.99
25	-	-
26	Ne	6074.34
27	-	-
28	Ne	6096.16
29	Ne	6120.45
30	Ne	6143.06
31	Ne	6163.59
32	Ne	6217.28
33	Ne	6266.50
34	Ne	6304.79
35	Ne	6334.43
36	Ne	6382.99
37	Ne	6402.25
38	Ne	6506.53
39	Ne	6532.88

Ref. #	Source	λ_{lab}
1	Ne	5330.78
2	Ne	5341.09
3	Ne	5400.36
4	Ne	5562.77
5	Kr	5570.29
6	-	-
7	Ar	5650.70
8	-	-

Within the blue-violet region, ten pairs of lines were selected randomly. For each pair, a reciprocal dispersion was calculated. The accepted value was taken to be the average of the ten resulting D values. The reciprocal dispersion of the red region was obtained by the same method.

For the blue-violet region

$$D = 84.04 \pm 0.08 \text{ (s.d.) } \overset{\circ}{\text{A}}/\text{mm.}$$

For the red region

$$D = 84.06 \pm 0.09 \text{ (s.d.) } \overset{\circ}{\text{A}}/\text{mm.}$$

Average reciprocal dispersion for the two regions

$$D = 84.05 \pm 0.09 \overset{\circ}{\text{A}}/\text{mm.}$$

iv) Adopted Camera Focus Settings

(using grating BL 280)

With the identification of the comparison lines, the focus test plates were visually examined to determine the best focus settings at specific wavelengths. The best settings were found to be the following:-

2.98	at	4200 $\overset{\circ}{\text{A}}$
2.83	at	4500 $\overset{\circ}{\text{A}}$
2.83	at	5300 $\overset{\circ}{\text{A}}$
2.74	at	5800 $\overset{\circ}{\text{A}}$
2.68	at	6500 $\overset{\circ}{\text{A}}$

IV

PRODUCTION OF STELLAR SPECTROGRAMS

1) Spectrograph Operating Settings

Assuming the operating settings obtained from the comparison spectrum test plates were useable for stellar spectroscopic work, the early stellar plates involved the testing of these settings and estimates of exposure times. A number of stars of various magnitudes were selected from a list of MK standards. A spread of exposure times were estimated for each star based on their blue magnitude. The settings from the focus plates were tested on these stars and were found satisfactory for stellar work. All stellar spectra were photographed using decker position 3.

The focus setting of 2.98 gave sharply focused spectrograms with the exception of the region of $\lambda < 3900 \text{ \AA}$. Within this region, lines appeared to quickly fall out of focus with decreasing wavelength. As this region is not critical for stellar classification, the lack of focus within this zone was considered to be unimportant. Based on the sharp appearances of the absorption lines within the region from 4000 to 4600 \AA , the 2.98 setting was adopted as the focus for MK classification.

The grating tilt setting of 1.10 was found satisfactory for stellar work, placing the spectra centrally on the plate.

The slit setting of 1.5 ($1.8''$) was found to be wide with respect to the stellar images on the slit jaws, and hence the trailing process for all but the brightest stars was difficult. The slit setting was reduced to 0.5 ($0.7''$) to eliminate this problem. Comparison of plates using both slit settings showed that the reduction to 0.5 acted to slightly improve the resolution of the spectrograms. A further reduction in slit width was considered, but careful examination of the spectrograms obtained with the 0.5 setting showed sufficient resolution (a projected slit width of 0.5 \AA) for stellar classification.

From the stellar spectrograms, the best exposure time for each star was selected. This was obtained by matching the appearance of the produced spectrograms to those of the Abt-Meinel Atlas (1968), where appearance refers to the clarity and sharpness of the absorption lines and the darkness of the continuum. Using these exposure times and the stellar magnitudes, a curve of m_B versus exposure time was constructed. (Figure 4). This curve should be representative of average ($1 - 2''$) seeing conditions in Halifax.

By using an optical density of 0.90 and considering exposure times as being inversely proportional to luminosity, predicted exposures with the neutral density filter were calculated from Figure 4. An exposure curve (Figure 5) was constructed from these calculated values. The curve was then verified with spectra exposures taken with the filter. It is

recommended that the filter be used for stars of blue magnitude brighter than 3^m0 . A star of $m_B = 3^m0$ without the use of the filter requires an exposure time of 30 seconds which corresponds to only one trail. Using the filter increases the exposure to 3.5 minutes. Increasing the exposure and hence, the number of trails, ensures a more uniformly - exposed spectrogram.

Figure 4

Exposure versus apparent magnitude relation for the classical spectrograph. Grating BL 280; Slit 0.5 (0.7^{''}). The straight line was obtained by a least squares fit to the plotted points.

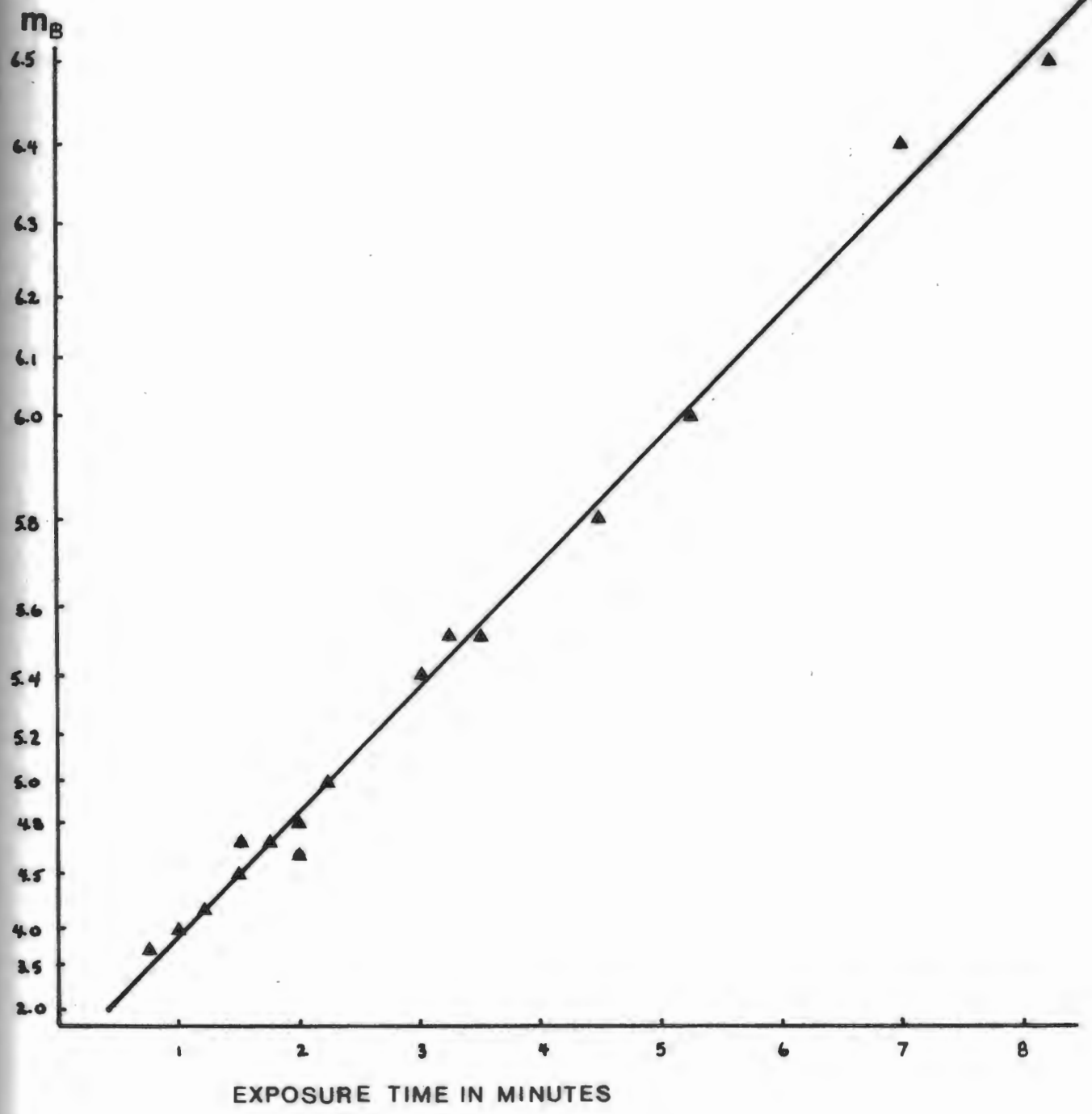
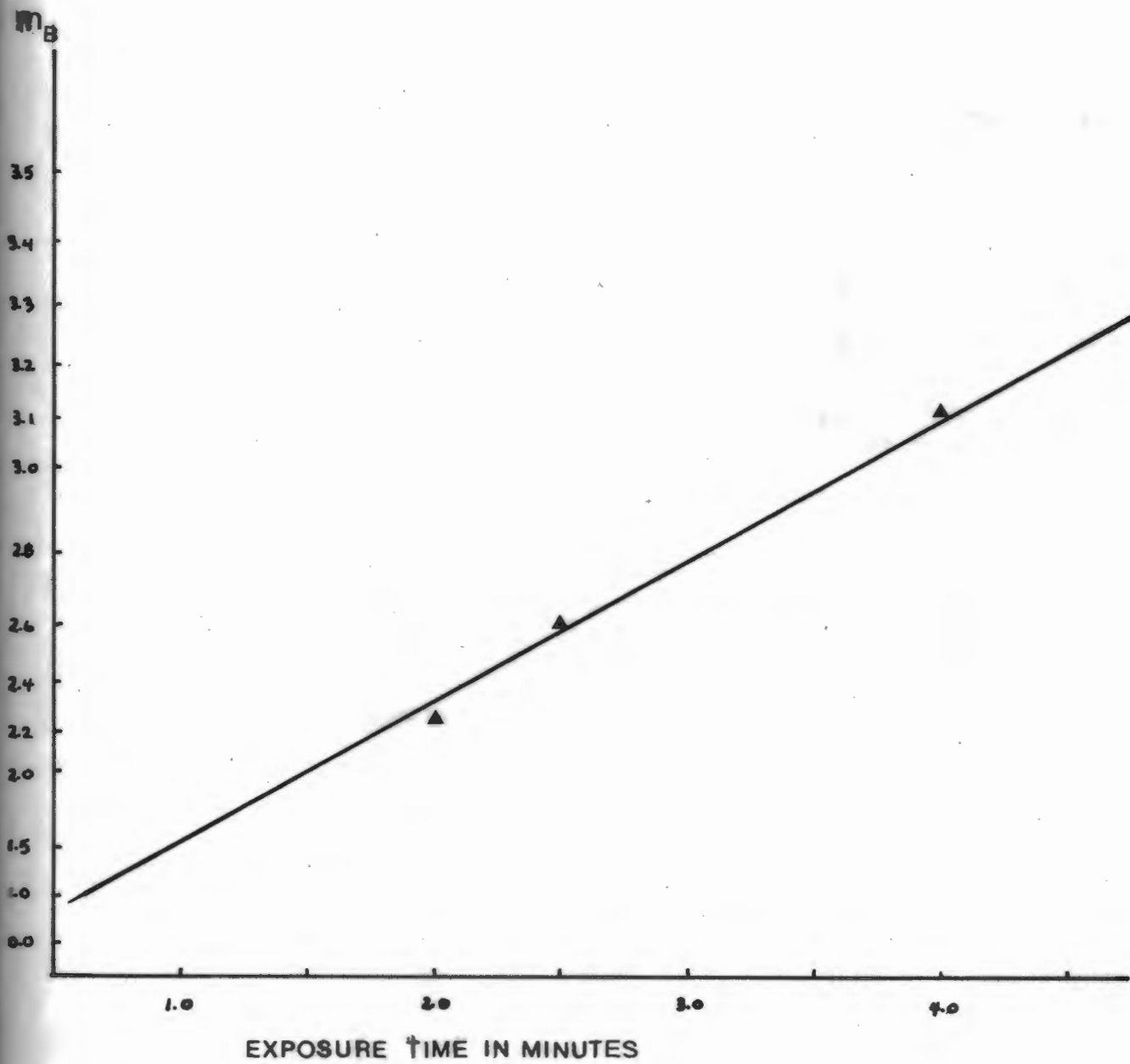


Figure 5

Exposure versus apparent magnitude relation for the classical spectrograph using the 0.90 optical density filter. Grating BL 280. Slit - 0.5 (0.7^{''}). The straight line was obtained from calculations using exposure times from Figure 4.

Fig 5, p22



ii) Spectrograph Operating Procedure

The procedure adopted for photographing stellar spectra is that outlined on pages 37 - 39 of the instruction manual 'The Spetz "Toy" Spectrograph at McGraw - Hill Observatory (Mook, 1975)'. Slight changes in the procedure were required to correct for wording misprints and mistakes. The Dome copy of the manual has been corrected.

The manual recommends that the comparison lines be placed on the plate in two exposures of one-half the total duration, and be photographed beside each stellar spectrum. These two steps were not considered necessary for the production of an MK atlas. In general, comparison spectra were applied only on the top and bottom of each plate to act as a quick reference for the identification of the major spectral lines (G Band, H and K lines, Balmer Series)

As suggested in the manual, the spectrograph slit was aligned east - west and the trailing process was performed using the guide speed R.A. controls. The length of trailing times depended on the stars' declination and varied from 20 seconds at $\delta = 0^\circ$ to approximately 45 seconds at $\delta = 60^\circ$. All spectra were photographed using the # 3 decker position (length = $54''$ on the sky, or 0.40 m.m. on glass).

Stars were trailed only in a whole number of passes along the slit to prevent non-uniform exposures.

iii) Exposure Curve Recalibration

During the period of July - October 1977, the exposure curves (Figures 4 and 5) gave reliable exposures for stellar spectra. However, on returning from a two month absence from observing, the result of adverse weather during November and early December, the exposure curves were found to be no longer valid. Several plates taken during the months of December and January using exposures taken from these curves were found to be significantly underexposed.

Initially some defects within the spectrograph were suspected. The instrument was dismantled in search of the problem. The light path was followed through the interior of the spectrograph checking for any form of light blockage that might act to increase the exposure times; but none was found.

The slit width dial calibration was remeasured with the Gaertner engine to check the possibility that it had changed. If the 0.5 setting was now giving a narrower slit than previously, less of the stellar light would be admitted into the spectrograph resulting in underexposure. However, measurements confirmed the previous calibration, disproving this hypothesis.

The spectrograph grating was also examined. The grating surface was found to be covered with a poorly reflecting film along with a number of fine scratches. The film may be due to the oxidization of the aluminum surface coating of the

grating. The scratches were attributed to a fine-hair lens brush which had been used to clean the grating surface. At this time, it is uncertain to what extent the scratches have actually damaged the grating surface.

The telescope optics were also checked. The primary mirror which was recoated and cleaned during the summer of 1977, was clearly in need of resurfacing by early 1978. The mirror was removed from the telescope and washed, but no improvement in the exposure time resulted.

It was concluded that the underexposed plates were the result of the deterioration of both the mirror and grating surfaces. To test the effect of the degraded grating surface, test plates of various exposures of the comparison spectrum were obtained. In comparing these plates with ones taken during July and August 1977, the grating appeared responsible for a sensitivity loss factor of about 3, in that a 20 second exposure on the early focus test plates now corresponded to a 60 second exposure. Estimating a factor of 2 for the primary mirror alone implied that the original exposure curve had to be recalibrated towards longer exposures by a factor of approximately 6.

To carry out the recalibration, plates of MK standards were taken using a wide range of exposures centered about the estimated factor of 6. Shown in Table 3 are the results.

The recalibration factor was found to vary from 6.7 to 10.5 with an average of 8.6. A relationship between the factor and the star's blue magnitude was found to exist in that as the stars became fainter, the factor increased. To illustrate this observation, Figure 6 was constructed. As the 34 minute exposure time for 31 Com. produced a slightly underexposed spectrogram, the plotted point for this star must be considered as a lower limit. One possibility for the observed effect shown in Figure 6 is reciprocity failure. This was confirmed as being partially responsible by checking the 103 a-0 reciprocity characteristics provided by the Kodak Company.

Until a new grating is available and the telescope mirror is resurfaced, it is recommended that the exposure times from Figures 4 and 5 be increased by either the mean factor of 8.6 or the appropriate factor obtained from Figure 6. With the continuing deterioration of the mirror and grating surfaces, it is possible that the recalibration factor may continue to increase with time.

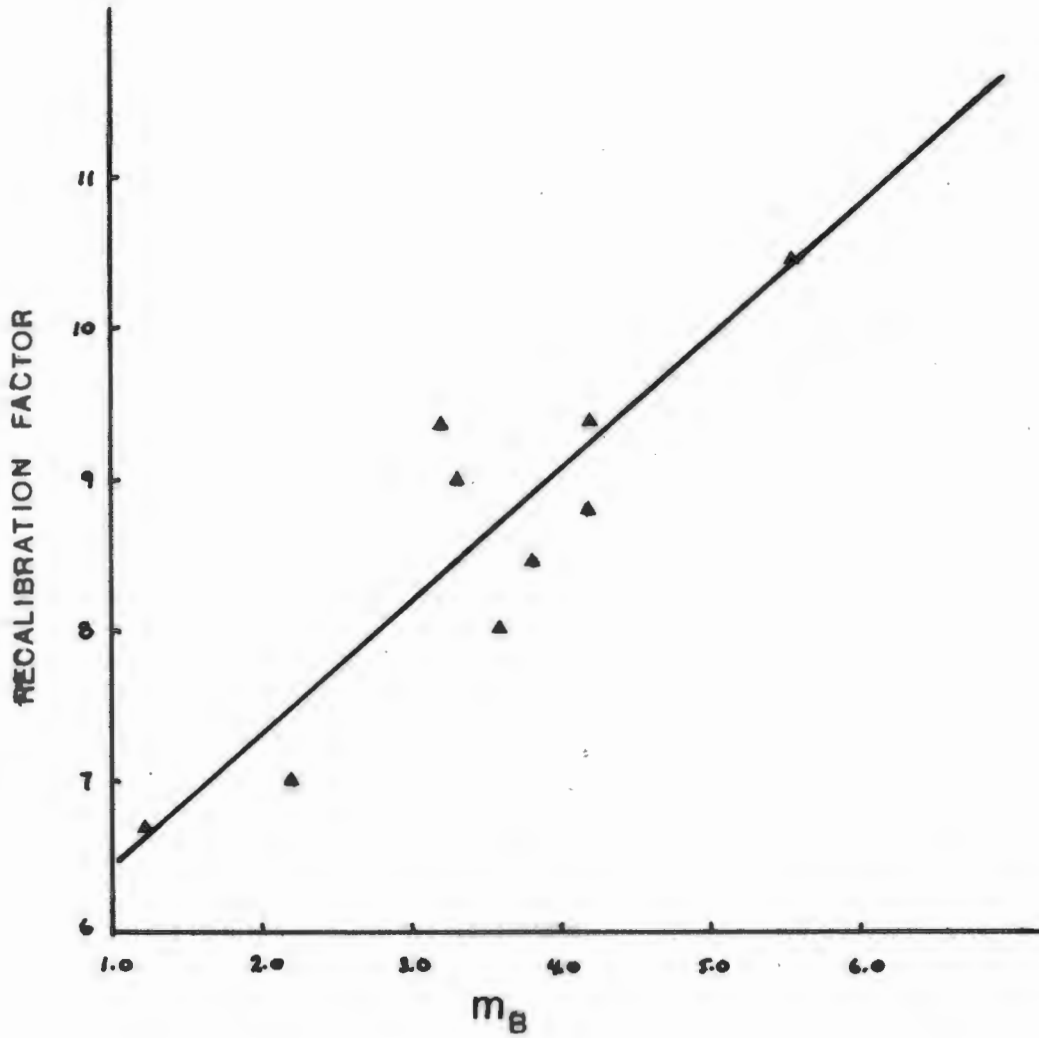
Table 3 Exposure Curve Recalibration

Star	Blue Magnitude MB	Original Exposures (Fig. 4 and 5) Valid For July - Oct 77	New Exposures Period Jan 78 To Present	Empirical Recalibration Factor
α Leo	1.2	45 sec (Filter)	5.0 min (Filter)	6.7
β Leo	2.2	15 sec.	1.75 min.	7.0
γ U. Ma.	3.3	40 sec.	6.0 min.	9.0
δ Dra.	3.6	45 sec.	6.0 min.	8.0
ϵ Boo.	3.2	40 sec.	6.25 min.	9.4
ζ U. Ma.	4.2	1.25 min.	11.75 min.	9.4
η Leo	3.8	55 sec.	7.75 min.	8.5
θ U. Ma.	4.2	1.25 min.	11.0 min.	8.8
31 Com.	5.5	3.25 min.	34.0 min.	10.5

Figure 6

A plot of the exposure curve recalibration factor versus blue magnitude (constructed from the data shown in Table 3). The straight line was applied to the plotted points by a least squares fitting method.

Fig 6, P 28



PRODUCTION OF AN MK CLASSIFICATION ATLAS

i) Selection of Program Stars

With the testing of operating settings and exposure times completed, plates of stellar spectra were taken with the aim of producing an MK classification atlas for the giant (III) and main sequence (V) luminosity classes. Ideally, the atlas would include a spectrogram of each spectral type for each luminosity class. The lack of suitable standard stars for certain spectral classes and the large amount of observing time required made it impossible to produce such an atlas. The sequence of stars and the spacing of spectral classes shown in the "Atlas of Low Dispersion Grating Stellar Spectra" by Abt, Meinel, Morgan, and Tapscott (1968), and "An Atlas of Spectra of the Cooler Stars, Types G, K, M, S, and C" by Keenan and McNeil (1976) were used as guides in the selection of suitable program stars. Program stars were also selected from the lists of MK standards given in Johnson and Morgan (1953), and, Morgan and Keenan (1973). Where gaps in the spectral sequence existed that could not be filled with MK standards from the above lists, stars were selected from the Catalogue of Bright Stars, Third Edition, 1964.

ii) Darkroom Processing

All plates were obtained on Eastman - Kodak 103a - 0 emulsion (catalogue number 170 - 8932) and were developed

in D - 19 for four minutes at a temperature of 70 - 73° F. An attempt was made to produce contact copies using 103a - 0 emulsion on glass. This proved unsatisfactory due to graininess and the non uniformity of the plate background. The non uniformity, which occurred near the plate edge, was attributed to the securing tabs of the plateholder interrupting the flow of developer over the plate. In general, this non uniformity did not impair the use of the originals or the contact copies. The grainy texture of the background became more noticeable when paper prints of these contact copies were produced. In order to avoid the above problems, contact copies were made using fine - grained Kodak Panatomic - X film (ASA 32). This film was developed in the Nikor tanks instead of the plateholder, eliminating the background irregularity. Use of this film also reduced the background graininess. Paper prints of these contacts were made using Kodak Polycontrast Rapid R.C. paper. No contrast filters were necessary in this step.

iii) MK Atlas

From the paper prints, spectrograms were selected and arranged in order to illustrate the MK spectral types for the main sequence and giant luminosity classes. Tables 4 and 5 list the sequence of stars and the observational data for the BGO atlas. It is emphasized that the Atlas in paper print form is not intended to be used for the most accurate classification work. For this purpose, only the original glass plates listed in Tables 4 and 5 are suitable.

iv) Atlas Plates 1 and 2

Plates 1 and 2 illustrate an array of MK standards for the main sequence and giant luminosity classes. The sequences of the two plates show the changing appearances and intensities of lines, blends, and bands which allow the classification of luminosity class III and V stars.

Plate 1 commences the sequence with an O9 V spectrogram which shows numerous H and He lines. The hydrogen lines increase in intensity with advancing spectral type reaching their maximum strength near A0 V. The HeI lines reach maximum strength near B3V and decrease in intensity thereafter. The CaII K line which can be used for classification as early as B8V as shown in the Abt - Meinel Atlas, is not clearly seen on the BGO glass plates until A3V and is faintly observable at A0V. This is due to the rapid change in focus between the position of this line and that of best focus (4200 Å). The net result is a slight increase in uncertainty in assigning spectral classes within the range of late B and early A stars. The K line beyond A0V increases rapidly in intensity with later types. Within the sequence A0V to F5V, the CaII K to H δ line ratio changes noticeably with spectral type and the neutral metallic lines grow in strength. The G Band begins to appear as a continuous feature near F3V. The sequence between F5V to K0V is characterized by decreasing H lines and by increasing neutral metallic lines. The G Band increases in strength towards the late G classes. The KV stars

reveal a G Band which decreases in intensity and a CaI 4226 line which rapidly strengthens with advancing spectral type. The late K classes are marked by the appearance of an MgH absorption band centered at 4780 Å.

Plate 2 reveals a similiar pattern of changing line and band intensities. The B2III spectrogram shows the Balmer line series and several helium lines. Towards later classes, the H lines grow in intensity reaching a maximum near A0III, while the He lines which are near maximum strength near B2III, decrease in intensity. The Balmer lines of plate 2, as expected, based on pressure broadening theory, show more clearly defined edges and narrower appearances than do the same lines of the corresponding spectrograms shown in plate 1. Within the region of A0III to F6III, the H lines continue to weaken while the K line strengthens. The G Band is first seen as a continuous feature at F6III, and grows in intensity with later classes throughout the F and G giants. The neutral metallic lines strengthen progressively through the sequence F6III - K0III. Within this region, the CN absorption band and the 4172 - 4179 band are seen. The K and M stars reveal a weakening G Band and a rapidly increasing Ca I 4226 line with advancing spectral types. The TiO Bands grow noticeably in strength after K7III.

The above discussion of lines, blends, and bands forms the basis on which stars are assigned spectral classes. These features were described as they appear on the original glass plates. The ability of these plates to assign accurate class-

Table 4 Atlas Sequence of Main Sequence Stars (Plate 1)

Spectral Class	Name	α (1977)	δ (1977)	MB	Plate no.	Date	Exposure Time
O9	10 Lac. 1	22h 38	38° 56	4.7	C-023	7 Sept 77	1.75 min.
B3	1 Her. 1	17h 39	46° 01	3.6	C-012	31 Jul 77	40 sec.
B7	α Leo. 1	10h 07	12° 05	1.2	C-027	2 May 78	5.0 min. (f)
B9	α Del. 1	20h 39	15° 50	3.7	C-015	15 Aug 77	50 sec.
A0	γ Oph. 1	17h 47	2° 43	3.8	C-017	25 Aug 77	50 sec.
A3	β Leo. 1	11h 48	14° 42	2.2	C-028	5 May 78	1.75 min.
A5	80 U. Ma. 1	13h 24	55° 06	4.2	C-031	10 May 78	11.0 min.
A7	1 U. Ma. 1	8h 58	48° 10	3.3	C-028	5 May 78	6.0 min.
F0	ρ Gem. 1	7h 28	31° 50	4.5	C-030	8 May 78	12.0 min.
F3	ζ Ser. 1	17h 55	-3° 41	5.0	C-022	7 Sept 77	3.0 min.
F5	17 Cyg. A1	19h 46	33° 41	5.5	C-018	25 Aug 77	3.25 min.
F6	110 Her. 1	18h 45	20° 32	4.8	C-018	25 Aug 77	2.0 min.
F8	ϵ Dra. 1	16h 02	58° 37	4.5	C-018	25 Aug 77	1.50 min.
G0	72 Her. 1	17h 20	32° 31	6.0	C-018	25 Aug 77	5.25 min.
G2	16 Cyg. A1	19h 41	50° 29	6.5	C-022	7 Sept 77	9.0 min.
G5	16 Cyg. B1			6.9	C-024	9 Sept 77	15.0 min.
K0	σ Dra. 1	19h 32	69° 39	5.5	C-019	29 Aug 77	3.50 min.
K3	HR 88321	23h 12	57° 02	6.6	C-023	7 Sept 77	9.50 min.
K5	61 Cyg. A1	21h 05	38° 33	6.4	C-022	7 Sept 77	7.25 min.
K7	61 Cyg. B1			6.7	C-024	9 Sept 77	18.5 min.

NOTE:-

1. For Tables 4 and 5, the number beside each stellar name indicated the reference source from which the star was selected.
 1. - original MK system
 2. - the MK† system
 3. - catalogue of Bright Stars, Third Edition

Table 5 Atlas Sequence of Giant Stars (Plate 2)

Spectral Class	Name	α (1977)	δ (1977)	M_B	Plate No.	Date	Exposure Time
B2	β Cep. 3	21h28	700 28	3.0	C-022	7 Sept 77	3.50 min.
B6	δ Dra. 3	17h09	650 44	3.1	C-021	1 Sept 77	4.0 min. (f)
B9	γ Lyr. 1	18h58	320 39	3.1	C-011	31 Jul 77	30 sec.
A0	α Dra. 1	14h04	640 29	3.6	C-030	8 May 78	6.0 min.
A5	α Oph. 1	17h34	120 35	2.2	C-021	1 Sept 77	2.0 min (f)
A7	γ Boo. 1	14h31	380 24	3.2	C-030	8 May 78	6.25 min.
F0	δ Leo. 1	10h15	230 31	3.8	C-031	10 May 78	6.50 min.
F6	HR 65773	17h38	130 21	6.6	C-022	7 Sept 77	10.0 min.
G0	31 Com. 1	12h51	270 30	5.5	C-031	10 May 78	34.0 min.
G5	0 U. Ma 2	8h29	600 47	4.2	C-031	10 May 78	10.0 min.
G7	ϵ Dra. 2	19h48	700 13	4.7	C-024	9 Sept 77	2.25 min.
G9	K Cyg. 2	19h17	530 19	4.7	C-017	25 Aug 77	1.75 min.
K0	ϵ Oph. 2	16h13	-40 27	4.2	C-014	15 Aug 77	1.25 min.
K2	109 Her. 2	18h23	210 45	5.0	C-014	15 Aug 77	2.25 min.
K5	γ Dra. 1	17h56	510 29	3.7	C-017	25 Aug 77	45 sec.
K7	29 Her. 2	16h32	110 32	6.4	C-014	15 Aug 77	7.0 min.
M1	106 Her. 1	18h19	210 54	6.5	C-014	15 Aug 77	8.0 min.
M2	55 Peg. 1	23h06	90 17	6.1	C-023	7 Sept 77	5.5 min.
M3	32 Oph. 2	17h02	140 07	6.5	C-014	15 Aug 77	8.0 min.
M6	30 ϵ Her. 1	16h30	410 56	6.7	C-014	15 Aug 77	8.0 min.

NOTE:-

- 2 Exposure times marked by (f) indicate that the 0.90 neutral density filter was used.
- 3 The long exposure time for 61 Cyg B (K7V) was necessary due to high thin cloud coverage.

PLATE I. MAIN SEQUENCE.

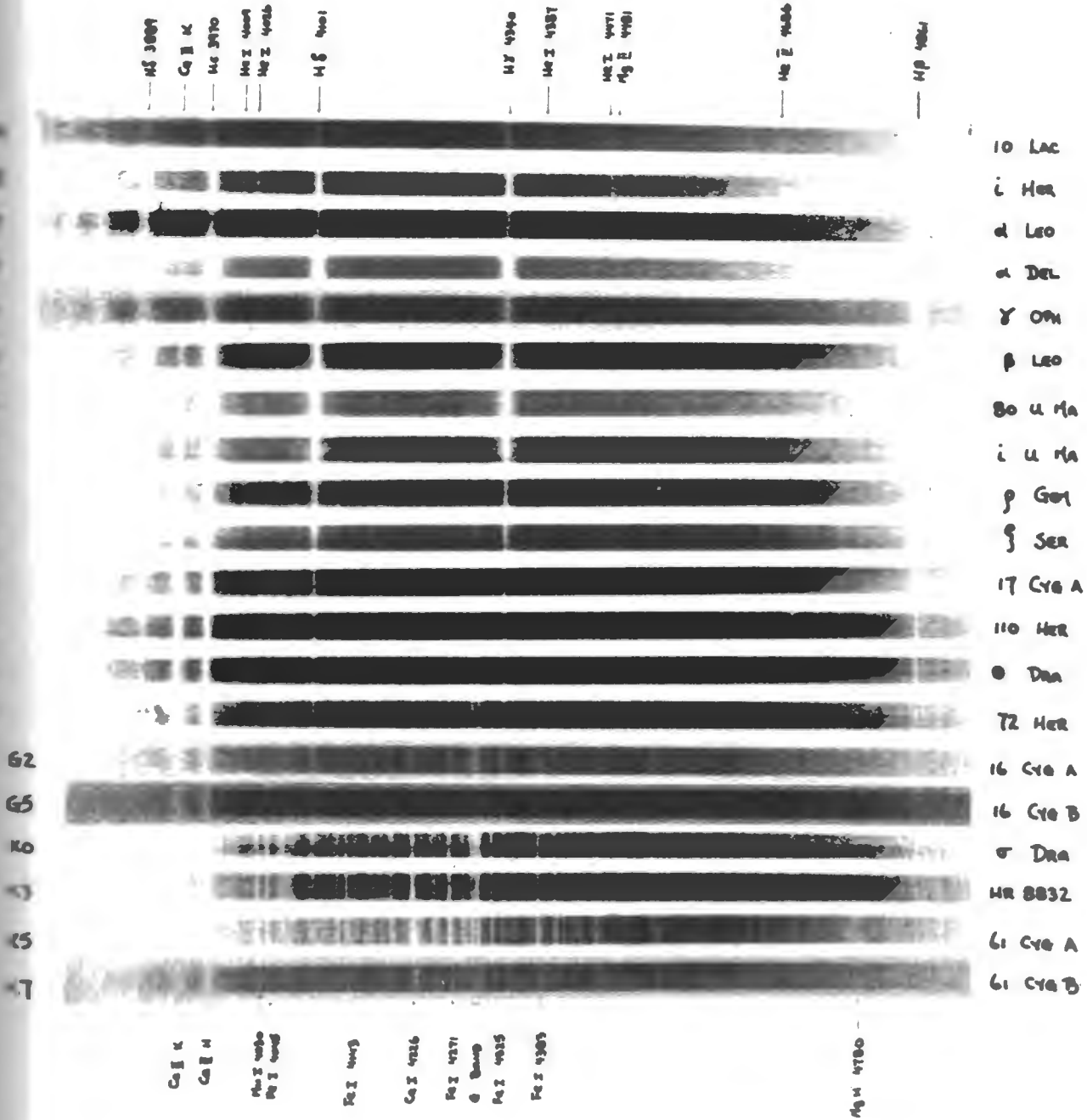
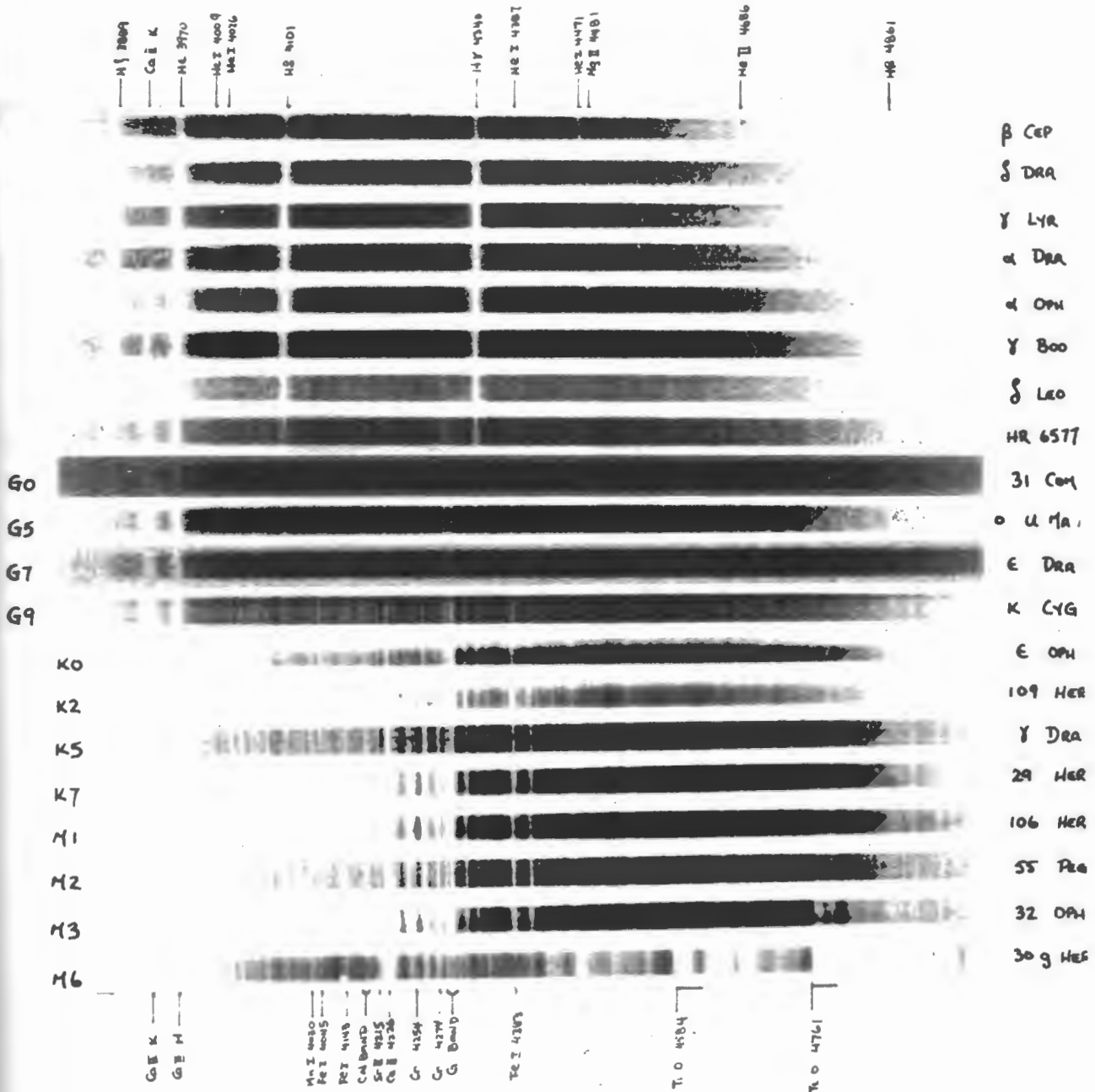


PLATE 2 Giant Stars.



ifications was tested, using stars which during these tests, were of unknown classes.

v) Classification of Unknown Spectra

With the atlas, the capacity to classify unknowns by luminosity class is limited. To remove this restriction, it is essential that the atlas be supplemented with a sequence of supergiant stars. Also, within the atlas, there exist several noticeable gaps. To improve the classification capacity of the BGO atlas, these gaps must be filled.

For the main sequence stars, the most noticeable weakness is the absence of any M star spectrograms. Sufficient M V standard stars are listed in Table 3 of "An Atlas of Spectra of the Cooler Stars" by Keenan and McNeil (1976) and in Table 3 of Johnson and Morgan (1953) to complete this region of the atlas. However, the faintness of these stars (all with $m_B > 8^m$) requires lengthy exposure times. With a freshly resurfaced mirror and a new grating, extrapolation of Figure 4, ignoring reciprocity failure, yields exposures of approximately 35 and 80 minutes, respectively, for stars of 8^m and 9^m . With the deterioration of the grating and mirror surfaces, Figure 6 indicates that these exposure times must be lengthened by a factor of 12 or 13. These very long exposures prevented the completion of this region of the atlas.

A second gap exists between G5V and K0V. Both the Atlas of Spectra of Cooler Stars and the Abt - Meinel Atlas

have filled this gap with 61 U Ma (G8V) which (with co-ordinates of $\alpha = 11^h 39^m$ and $\delta = 34^{\circ} 20'$ and $M_B = 6^m 0$) is obtainable with a 60 minute exposure time. This time was obtained from Figure 4 and by applying a recalibration factor of 11. This does not include allowance for reciprocity failure.

For the giant stars, the atlas possesses certain regions which could be improved by a closer spacing between spectral classes. The atlas sequence between F0III and G5III with only four members is not adequately filled. The poor coverage is caused by the lack of suitable standards as the Hertzsprung Gap extends through the F to middle G giant classes. The giant sequence could also be strengthened with the addition of an O III and early B III stars.

vi) Classification of Unknown Program Stars

A list of program stars was presented to the author to test the classification accuracy of the spectrograph and the BGO atlas. The author played no part in the selection of these stars and their classifications remained unknown to him until after the stars had been classified. These 11 program stars were photographed with both the classical spectrograph and with the image tube. Each star was classified twice, using its classical and image tube spectrograms. Only original plates were used, and in each case, the comparison was with the classical atlas described above. For a discussion of the image tube classifications, refer to Chapter 8. The assigned spectral

classes were then checked for accuracy with the classifications listed in the Catalogue of Bright Stars (Hoffleit, 1964).

In general, all the lines and features used by the Abt-Meinell Atlas for classification purposes are visible on the BGO Atlas and on the unknown spectrograms. For all 11 stars, the assigned spectral classifications differed by not more than 1 subclass from those listed in the Catalogue of Bright Stars.

Because of differences in pressure broadening, giant stars possess narrower spectral lines with more sharply defined edges than do main sequence stars of the same spectral type. This was particularly observable on the BGO plates for the Balmer (hydrogen) and helium (HeI) lines. This observation along with various luminosity discriminating line ratios (see below) provided the means of assigning luminosity types to the program stars. Seven of the 11 stars were assigned late B through middle A spectral classes. For these stars, luminosity classes were primarily determined by the appearances and widths of the Balmer lines. For the remaining four stars, which were assigned later spectral types, line widths and luminosity discriminators were employed. Those lines and line ratios which were used as luminosity indicators, included:

- 1) the CN Band for mid - G to mid - K giants,
- 2) the 4172 - 4179 band for F giants, and,

3) the ratios of (Fe I 4216 / Ca I 4226) and (Sr II 4077 / Fe I 4063) for late F, G, and early K stars.

The list of program stars and the classification results are given in Table 7 (page 59). Plates 3a and 3b show the classical and image tube spectrograms for each of the 11 stars. Overall, the BGO Atlas and the classification procedure yielded very good results. The assigned spectral types were all within one subclass of the accepted classifications and 9 out of the 11 stars were assigned the correct luminosity class.

VI

VARO IMAGE TUBE CAMERA

A second objective of this thesis involved testing the Spetz spectrograph with a Varo image tube to obtain the necessary operating settings and to examine the capacity of this combination for spectral classification. Listed below are the specifications of the image tube.

i) Description:-

40 m.m. diameter, single stage image intensifier

Manufactured by Varo Electron Devices

Model Number 8605

ii) Power Supply

Applied Voltage (input) - 6.75 V. d.c.

Nominal operating Voltage (output) - 15,000 V.

The d.c. voltage was supplied by two, 6.75 V. Mallory Duracell Mercury batteries (type TR 135 R). To allow a gradual increase of the applied voltage up to the operating 6.75 V., a potentiometer of 250 ohms was employed with the power supply.

iii) General Manufacturers' Specifications

Tube Dimensions	-	40 m.m. input diameter
		32 m.m. useful output diameter
Magnification	-	0.94
Tube Gain	-	approximately 30 to 40

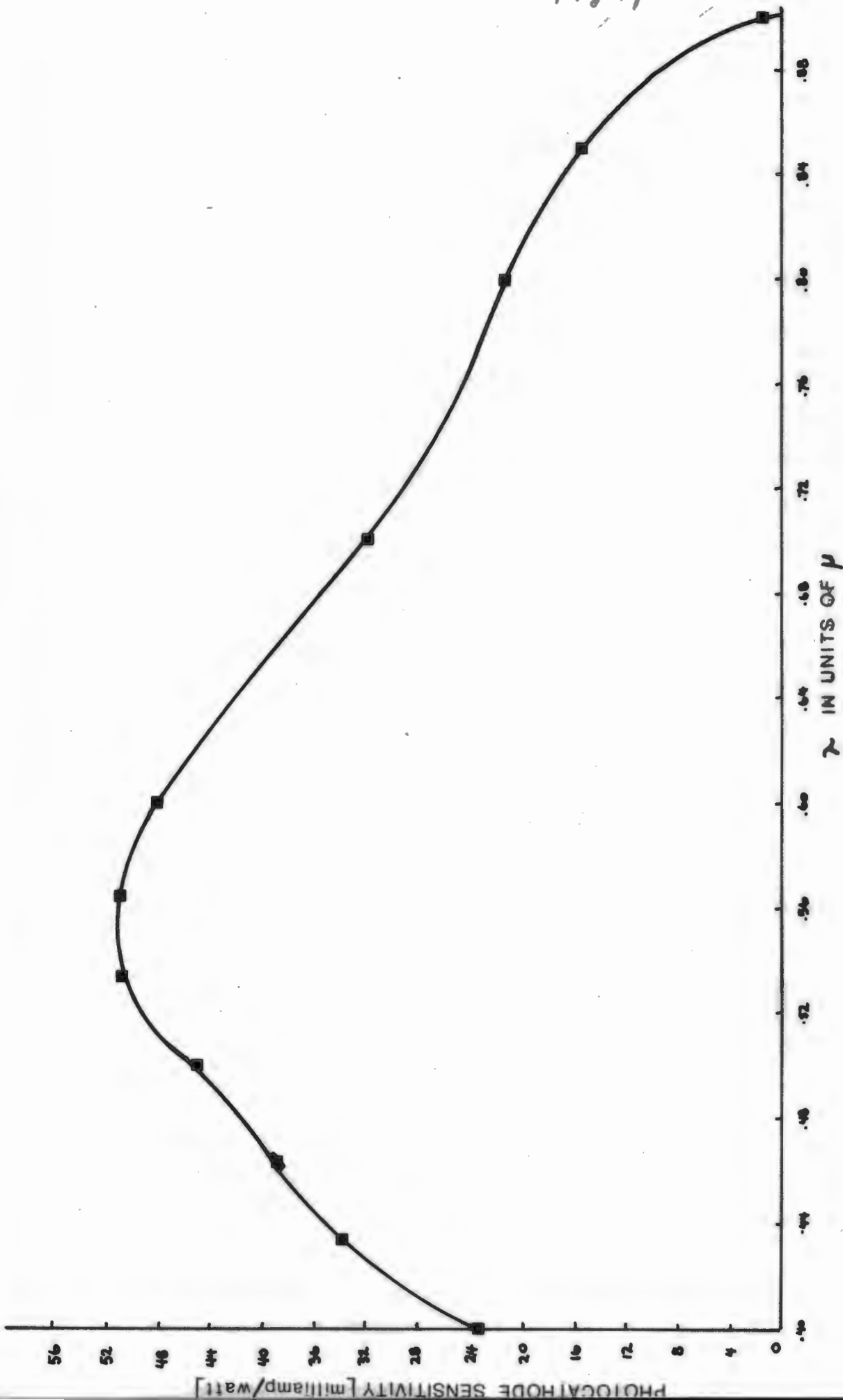
Focusing	-	electrostatic
Photocathode	-	S-20, with an extended red response
Phosphor	-	Aluminized P - 20
Output	-	Fiber Optics

Figure 7 shows the photocathode spectral response curve as provided by the Varo company.

Figure 7

The photocathode spectral response curve of the Varo image tube, model # 8605. The curve is fitted by eye to the plotted points.

Fig 7, P42



VII

IMAGE TUBE TESTING

i) Image Tube Operating Settings

As with the initial preparations of the classical spectrograph, a trial and error process of testing various operating settings was performed with the image tube camera using the comparison spectrum and 103a - D emulsion. The slit width dial setting was maintained at 0.5. The grating tilt setting was initially positioned at 1.10. The tilt setting was adjusted as necessary to center the comparison spectrum on the plate or to shift the spectrum to provide a more complete coverage of the red wavelength region. Based on the focusing test plates, a best focus of 7.60 and a comparison spectrum exposure time of 20 seconds with the neutral density filter were selected.

From these test plates, several facts were noted. The grating tilt setting of 1.10 provided coverage of the region 4250 - 5975 Å. All blue-violet lines at wavelengths shorter than 4250 Å were found to be very underexposed. Longer exposure times failed to improve this condition. The problem was attributed to the falling sensitivity of the image tube at these short wavelengths.

To extend the coverage of the red region, a tilt setting of less than 1.10 must be employed. A setting of 0.60 was later selected and provided a wavelength coverage from 4200 Å to 6550 Å.

The focusing test plates revealed a very gradual change in focus with camera focus settings. Focus settings of 7.50 and 7.70 provided results that were comparable to those at the 7.60 value. The slow focus change can be understood in terms of the lower resolution of the image tube plates. The focus setting of 7.60 was adopted for both the red and blue-violet regions.

ii) Reciprocal Dispersion

Using comparison spectrum # 1 of test plate IT # 2, the positions of 5 lines were measured with the Gaertner measuring engine. With these measurements and the known wavelengths of the comparison lines, the reciprocal dispersion of the plate was calculated and found to be the following:

- 1 $91.5 \pm 0.3 \text{ \AA} / \text{m.m.}$ for the blue - violet region
- 2 $65.5 \pm 0.2 \text{ \AA} / \text{m.m.}$ for the red region.

As the classical plates produced reciprocal dispersions of nearly identical values for these two regions, the wide spread found for the image tube plate was not expected. The difference between the two calculated dispersion values falls well outside of the tubes' maximum distortion of 5% quoted by the manufacturer.

It is apparent that the dispersion depends on the position of the comparison lines on the photocathode. To test this expectation, the comparison spectrum of plate I-002¹

1 Note that plates I-002 and IT #2 are not the same. I-002 refers to the second image tube plate of stellar spectra while IT #2 indicates the second image tube test plate of comparison spectra

which had been obtained with a different tilt setting, was used to remeasure the same set of five lines. The I-002 plate dispersions were found to be the following:-

- 1 $87.1 \pm 0.3 \text{ \AA/mm}$ for the blue-violet region
- 2 $82.6 \pm 0.3 \text{ \AA/mm}$ for the red region

The two plates (I-002 and I.T # 2) were obtained with a common focus of 7.60, a slit width of 0.5, and the same exposure of 20 seconds with the neutral density filter.

The sketches below show the rough locations of the red and blue regions of the comparison spectrum of each plate on the rear of the fiber bundle.

Plate IT #2 (24 Apr. 1978)

Slit - 0.5
Focus - 7.60
Tilt - 1.10

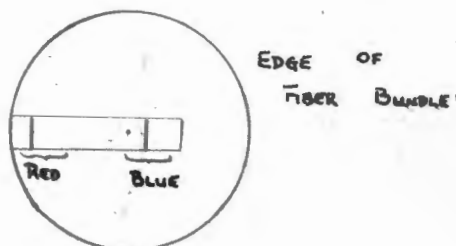
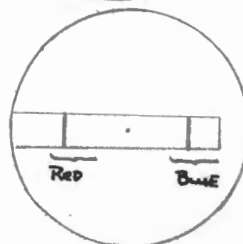


Plate I-002 (10 May 1978)

Slit - 0.5
Focus - 7.60
Tilt - 0.60



Based on the above information, it appears that the tube's dispersion varies with the location of the comparison lines on the photocathode. A change in the dc. applied voltage (6.75 V) might be expected to cause some distortion in the tube's dispersion. However, it does seem unlikely that the large dispersion differences could be explained by ageing of

the batteries during the 2½ week period between the two plates. The voltage was measured in early June and found to be 6.55 V.

From the plate I.T # 2 measurements, the following dispersions were adopted.

- 1 65 Å/mm for the outer plate edge, and
- 2 90 Å/mm for the central region of the photocathode

The 90 Å/mm dispersion value agrees with the 0.94 magnification of the tube.

VIII

PRODUCTION OF IMAGE TUBE SPECTROGRAMS

i) Introduction

The primary objective of this portion of the thesis was not to produce an MK atlas with the image tube but to test the classification capability of the instrument. This was accomplished by assigning classifications to program stars based on a comparison between their image tube spectrograms and the classical spectrograms which were used to produce plates 1 and 2. These tentative classes were then checked for accuracy against the accepted classifications listed in the Catalogue of Bright Stars (Hoffleit, 1964)

The procedure for photographing image tube spectra remained the same as that described previously for the classical spectrograph. All image tube photographs were obtained on Eastman - Kodak 103a-D emulsion (catalogue number 160-7860). Darkroom procedures were similar to those for the classical spectrograph process.

ii) Image Tube Exposure Times

With the operating settings obtained from the testing procedure, plates of stellar spectra were taken using a number of trial exposure times. The selection of trial times was based on the star's blue magnitude and Figure 4. The resulting exposure was adjusted by the appropriate recalibration factor and a tube gain factor of 30. The use of the recalibration factor was necessary as all image tube observations were obtained after the drop in system sensitivity.

The method of estimating image tube exposures described above, produced spectrograms which were very underexposed. Possible reasons for this are discussed below.

Using several exposures of longer duration, the same program stars were taken with the aim of producing an image tube exposure curve. Table 6 lists the program stars along with their apparent blue magnitudes and best exposure times. Using these tabulated values, the exposure curve (Figure 8) was constructed.

The image tube exposures were found to average 1.8 times longer than those given by Figure 4, the original exposure curve for the classical spectrograph. By considering the recalibration of this curve, a comparison between the recalibrated classical exposure times and the best image tube exposures for the program stars implies the tube gain in the blue-violet to be only 5, considerably less than the 30 to 1 gain quoted in the tube specifications. This may be explained in part by the falling sensitivity of the image tube at the blue-violet wavelengths (see Figure 7). A drop in the applied 6.75 V. would also cause a reduction in the tube gain. The battery voltage was measured in early June and a slight drop of 0.2 volts was found. To ensure a more steady power supply, it is recommended that for future image tube work, the batteries be replaced with a controllable d.c. power supply. Another factor causing the low gain is the 103a - D emulsion which is not as sensitive over the region of the out-

put of the P-20 phosphor as is 103a - 0 emulsion in the blue-violet region. Using the spectral sensitivity curves for these emulsions (provided by Kodak), the sensitivity difference was estimated to be a factor of three.

At the longer wavelengths (about 5600 \AA , the peak of the photocathode sensitivity curve; see Figure 7), the image tube gain could be expected to give a higher factor than the gain of 5 observed for the blue-violet region. This could be tested with classical and image tube test plates using the comparison spectrum and various exposure times.

iii) Image Tube Classification of Program Stars

As discussed in Chapter 5, a number of program stars were supplied to the author. The stars were photographed with the classical spectrograph and image tube camera. These stars were classified through comparison with the BGO Atlas glass plates and these assigned classes were then compared with published classifications.

As expected, based on the appearance of the comparison spectrum from the focus test plates and the sensitivity curve (Figure 7), the image tube produced stellar spectrograms which, for wavelengths of less than 4100 \AA , were considerably underexposed while the blue region ($4100 - 4800 \text{ \AA}$) was adequately exposed. The density in the violet region could be raised by lengthening exposure times but only at the expense of overexposing the blue wavelength region. The loss of the violet region which includes the Ca II H and K lines

Table 6 Image Tube Exposure Times
(Based on the Spectral Region 4100 - 4900 Å)

Program Star HD Number	mB	Original Exposure (Fig. 4)	Recalib. Classical Exposure	Image Tube Exposure	Image Tube Gain
129247	3.8	45 sec.	7.0 min.	1.5 min.	4.7
129502	4.3	1.25 min.	12.0 min.	2.25 min.	5.3
133208	4.5	1.5 min.	14.0 min.	2.5 min.	5.6
135742	2.5	20 sec.	3.25 min.	36 sec.	5.4
141003	3.7	45 sec.	7.0 min.	1.5 min.	4.7
149630	4.2	1.25 min.	12.0 min.	2.25 min.	5.3
153210	4.3	1.25 min.	12.0 min.	2.25 min.	5.3
159561	2.2	15 sec.	2.5 min.	25 sec.	6.0
164259	5.0	2.25 min.	22.0 min.	12.0 min.	-
165777	3.8	45 sec.	7.0 min.	1.75 min.	4.0
176437	3.2	40 sec.	6.25 min.	1.25 min.	5.0

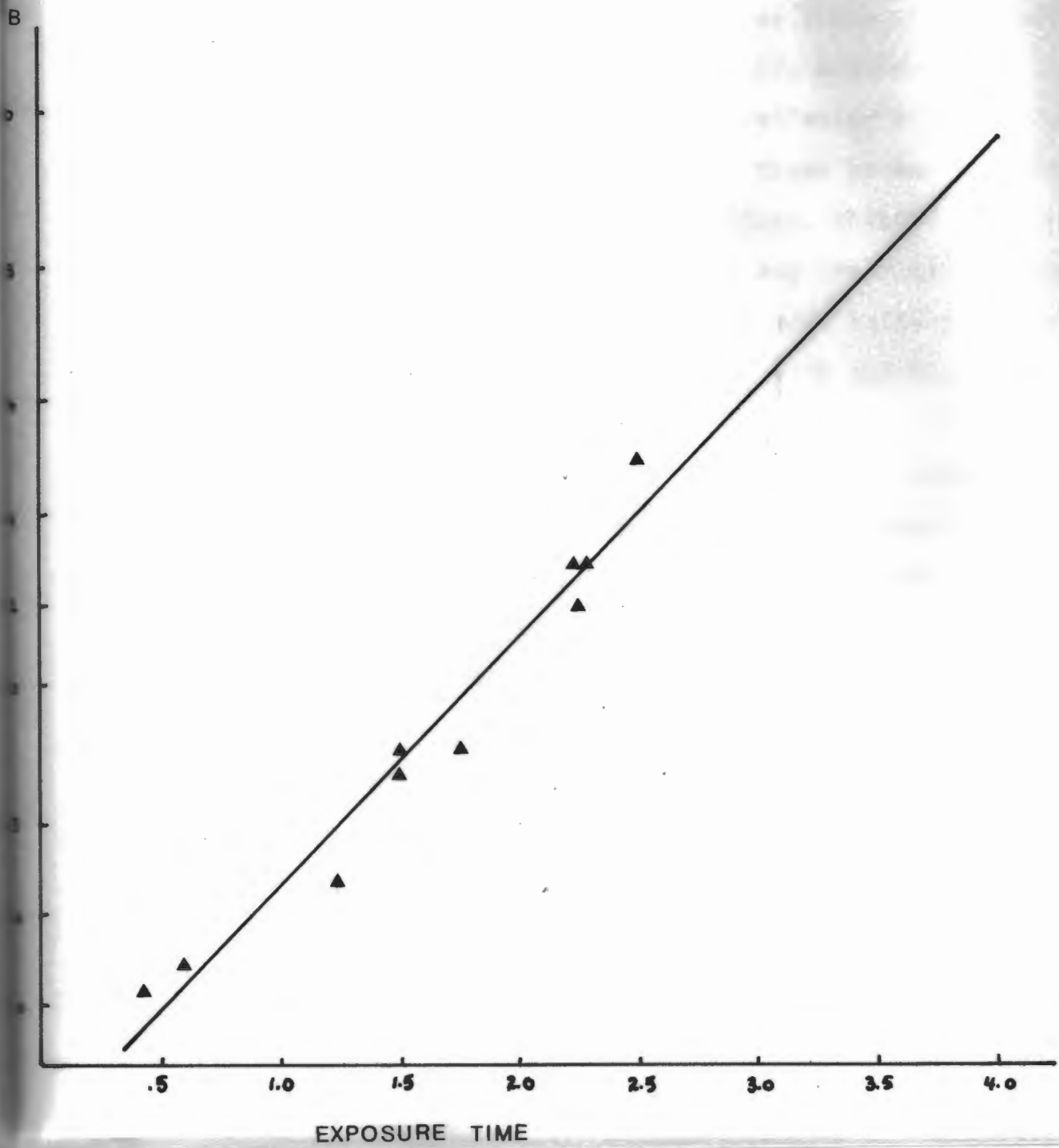
Average gain factor = 5.1

*Note:-

Although the image tube exposure curve (Figure 8) indicates a 4.25 minute exposure for this star, a 12 minute exposure was required due to a high thin cloud cover.

Figure 8

The image tube exposure curve. Slit 0.5 (0.7^μ).
Tilt - 0.60. 103a - D emulsion. D.C. voltage - 6.55 volts.
The straight line was fitted to the plotted points by a
least squares method.



is a major limitation in the classification of late B, A, and F stars. To the extent that classification within this region depends on the appearance of the Balmer lines, assigned classes must be considered as uncertain.

A close examination for Ca I (4226) and Mg II (4481) may be helpful in distinguishing between early and late A stars. If present in a spectrogram, these lines greatly assist the classification of stars later than A5. Similarly He I (4387 and 4471) lines allow the differentiation between early and late B stars. Stars of spectral types between B7 and A3, however, show only strong Balmer lines. Within this region, classes can not be assigned with any certainty. To improve the classification within this region, it is recommended that the BL 280 grating be replaced with one blazed at 4000 Å.

The image tube, as expected, produced lower resolution spectrograms, showing wider lines with unclear edges. The difference in line appearance between classical and image tube spectrograms made the assignment of luminosity classes uncertain. Plates 3a and 3b illustrate the comparison between the two spectrograms for the program stars.

For the image tube classification procedure, luminosity classes for the B and A stars were assigned primarily on the Balmer line widths and appearances. Considering the lower resolution of the image tube which acted to widen lines giving them unclear edges, care was necessary to avoid bias towards

assigning class V. The seven program stars which were assigned B and A spectral types were initially examined as a group to compare the Balmer line widths and appearances. The differences in widths among the group were used to assign luminosity classes. For those program stars given later spectral types, various luminosity discriminants were employed in addition to line widths.

To review the image tube classifications which are shown in Table 7, a summary of the classifying procedure for the 11 program stars follows.

a) HD 129247 (Spectrogram 4, Plate I-003)

Based on the strong Balmer lines, the star must fall close to A0. The absence of other lines prevents a firm classification but implies the star occupies the region B7- A3. The strong Balmer lines possess reasonably sharp, distinct edges, indicating luminosity class III.

b) HD 129502 (Spectrogram 5, Plate I-004)

Within this stellar spectrogram, the Balmer lines, a weak Ca I 4226 line, and a number of metallic lines including Mg II 4481, and Fe I 4383 are visible. The Balmer lines which are considerably weaker than those in HD 129247, possess edges which suggest a III classification. The combination and observed strengths of the hydrogen and metallic lines imply an early F star. (F2 III).

c) HD 133208 (Spectrogram 2, Plate I - 004)

This star shows a spectrum which is dominated by a wide,

strong G Band. Also present are several strong metallic lines including FeI 4325, FeI 4383, FeI 4271, and CaI 4226, along with weak Balmer lines. The portion of the spectrogram to the short wavelength side of CaI is underexposed. Based on the predominant G Band and the relative intensities of H δ and the nearby metallic lines, a spectral type of G7 was selected. The line ratio of (FeI 4216 / CaI 4226) indicates a luminosity class III.

d) HD 135742 (Spectrogram 3, Plate I - 006)

Strong Balmer lines and H ϵ are visible, implying a classification close to A0. Although the H ϵ line is seen, the Ca II K line was not present. The absence of the K line and any He I lines implies a late B star (B9 III).

e) HD 141003 (Spectrogram 2, Plate I - 006)

The spectrogram of this star is dominated by wide, fuzzy, strong Balmer lines. The only other observable line was found located close on the red side of the H line. This line was not observed on any of the Atlas spectrograms. The Abt-Meinell Atlas was used to identify this line as Si II 4128-4130 which appears in late B and early A stars reaching a maximum near A0. Using this information, the star was classified as A0V. Without this assistance from the Abt-Meinell Atlas, the BGO Atlas would have assigned a classification near A0V (ie within the region B7V - A3V).

f) HD 149630 (spectrogram 5, Plate I-006)

The presence of strong, wide Balmer lines and the absence of other observable lines implies a classification near A0V (ie within the range B7V- A3V).

g) HD 153210 (Spectrogram 2, Plate I-009)

Within this spectrum, a strong G Band, a weak H γ line, and metallic lines of FeI 4325, FeI 4383, CrI 4254, CrI 4274, and CaI 4226 are present. To the short wavelength side of the CaI line are several other faint features, one of which is believed to be the CN Band. The underexposed state of this region prevents any firm identification. Based on the strength of the G Band and the metallic lines, a classification of K0 III was selected. The giant class was based on the presence of the CN Band.

h) HD 159561 (Spectrogram 3 and 4, Plate I-009)

The combination of strong Balmer lines and a faint Mg II 4481 line coupled with the absence of the CaI 4226 line implies an early A spectral type. In order to obtain a more accurate classification, spectrogram 4 was obtained with twice the exposure time used for spectrogram 3. This spectrogram faintly showed both the H ϵ and Ca II K line. Using these lines, a classification of A5 III was selected.

i) HD 164259 (Spectrogram 2, Plate I-011)

This spectrogram shows the hydrogen lines of H β and H γ , and the Mg II 4481 line. Also there exists faint indica-

tions of the G Band. To the short wavelength side of the G Band, the spectrogram is underexposed and no lines are visible. Based on the above observations, a classification of F0 III was selected.

j) HD 165777 (Spectrogram 5, Plate I - 009)

Strong Balmer lines, the Mg II 4481 line, and a very faint Fe I 4383 line combine to indicate an early A spectral type. The appearance of the Balmer lines imply luminosity class V. The star was classified as A2V.

k) HD 176437 (Spectrogram 6, Plate I - 009)

This star was classified as B8 III based on the presence of strong Balmer lines which possess well-defined edges, a faint He I 4387 and He I 4026 line. The identification of the He I 4026 line remains uncertain due to the underexposed state of this region.

The assigned image tube classes are listed in comparison with the classically - determined, and the accepted catalogue classes. As expected, considering that the Atlas was produced with the classical spectrograph, the classically - assigned classifications showed a higher accuracy than did the image tube classifications. In spite of the image tube's loss of information at violet wavelengths and the reduction in resolution, the image tube classes were all within three subclasses of the catalogue classifications. Seven of the 11 program stars were assigned the correct luminosity class. In order to produce darker exposures in the violet region with-

out overexposing the blue wavelengths, it is recommended that the spectrograph's grating be replaced with one blazed at 4000 Å. Perhaps with the improvements resulting from this new grating, a classification atlas for the image tube system would be valuable. Clearly one would expect more accuracy in assigning classes using such an atlas than presently obtained by comparing image tube spectrograms to a classical atlas. However, considering the lower resolution, it seems unlikely that the accuracy of the image tube classification could match that of the classical system.

Table 7 Classification of Program Stars

Program Star HD Number	α	δ	MB	Assigned Image Tube Class.	Assigned Classical Class.	Listed Catalogue Class.*
129247	14 ^h 41	13° 43	3.8	A0 III (B7 - A3)	A3 III	A2 III
129502	14 ^h 43	-5° 39	4.3	F2 III	F3 V	F3 IV
133208	15 ^h 02	40° 23	4.5	G7 III	G9 III	G8 III
135742	15 ^h 17	-9° 23	2.5	B9 III	B9 V	B8 V
141003	15 ^h 46	15° 25	3.7	A0 V (B7 A0 V A3)	A2 V	A2 IV
149630	16 ^h 34	42° 27	4.2	(B7 - A3)	A0 V	B9 V
153210	15 ^h 58	9° 23	4.3	K0 III	K2 III	K2 III
159561	17 ^h 36	12° 34	2.2	A5 III	A5 III	A5 III
164259	18 ^h 01	-3° 41	5.0	F0 III	F3 V	F3 V
165777	18 ^h 07	9° 34	3.8	A2 V	A5 V	A4 V
176437	18 ^h 59	32° 41	3.2	B8 III	B8 III	B9 III

* from the Catalogue of Bright Stars, Third Edition, 1964.

PLATE 3a CLASSICAL (TOP) AND THREE TUBE (BOTTOM)
SPECTROGRAMS OF THE PROGRAM STARS

HD 129247
A2 III

H β 5889
Ca II K
H ϵ 3970
H δ 4101
H γ 4340
H δ 4861

HD 129502
F3 IV

Ca II K
H ϵ 3970
H δ 4030
H δ 4101
Ca I 4226
H γ 4340
Fe I 4383
H β 4481
H δ 4861

HD 133208
G8 III

H δ 4030
Fe I 4045
H δ 4101
Ca I 4226
Fe I 4271
G Band
H γ 4340
Fe I 4383
H δ 4861

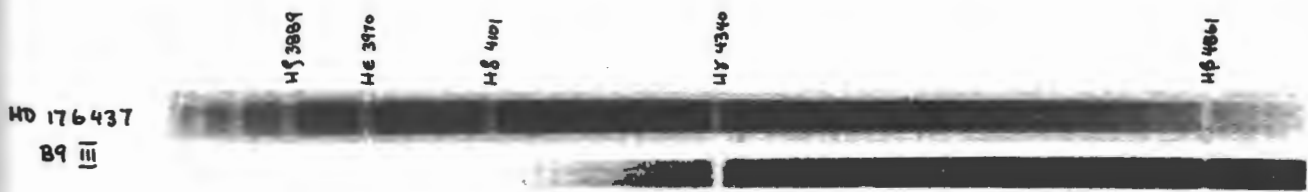
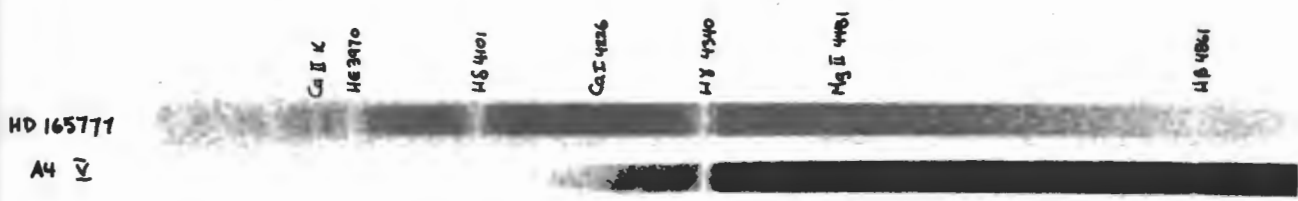
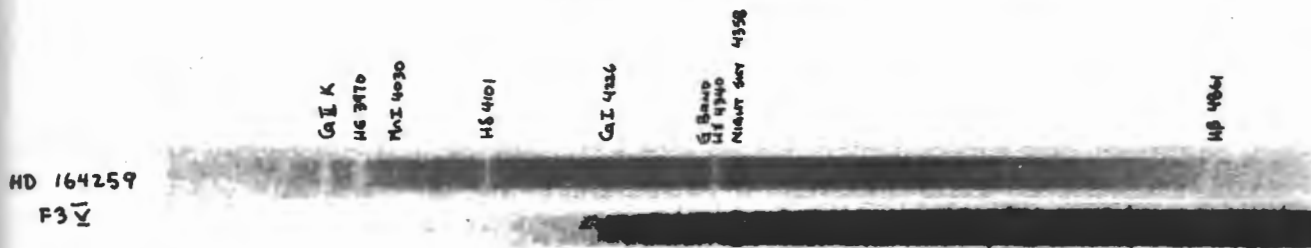
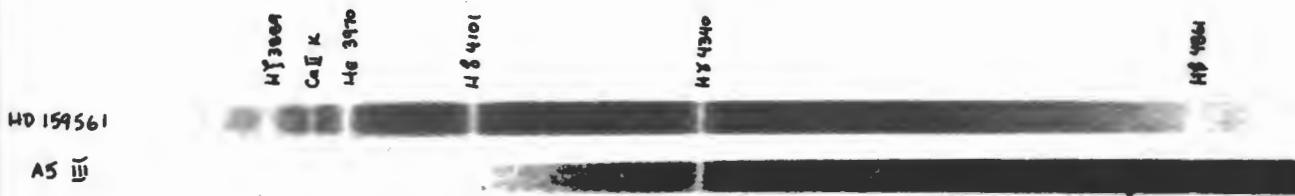
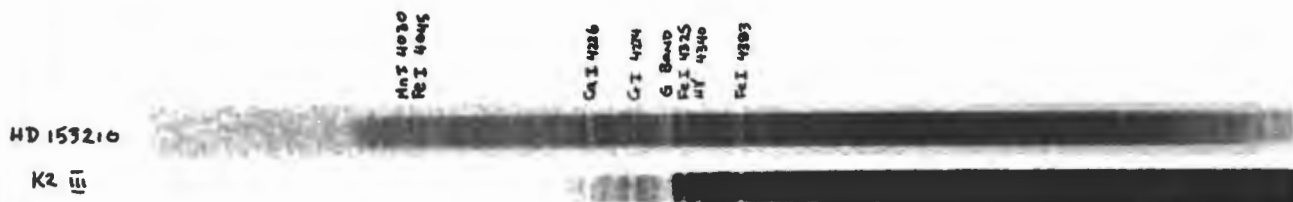
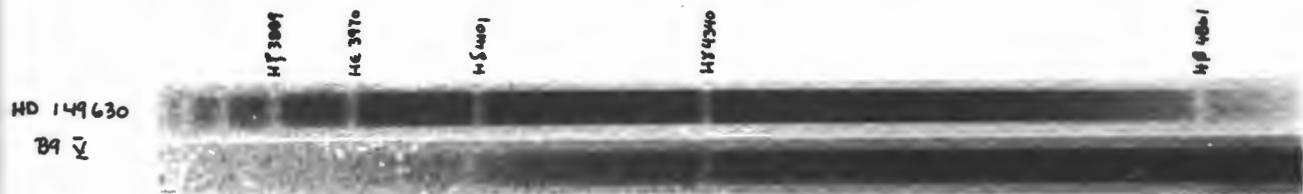
HD 135742
B8 V

H β 3889
H ϵ 3970
H δ 4101
H γ 4340
H δ 4861

HD 141003
A2 IV

H β 3889
Ca II K
H ϵ 3970
H δ 4101
H γ 4340
H δ 4481
H δ 4861

PLATE 3b CLASSICAL (TOP) AND IMAGE TUBE (BOTTOM)
SPECTROGRAMS OF THE PROGRAM STARS.



IX

SPECTRUM OF THE NIGHT SKY AT HALIFAX

i) Blue - Violet Region (3900 - 4700 Å)

The blue-violet region of the night sky spectrum was photographed at the zenith on 24 April 1978 using a 60 minute exposure (plate C - 025). The night sky spectrum is shown with the comparison spectrum in Figure 9. Due to the proximity of the Observatory to the Halifax Harbour Container Pier, which is continuously illuminated by mercury vapour lamps, the night sky spectrum was expected to show Hg I mercury lines. The mercury lamp spectrum provided by Osterbrook et al (1976) and the comparison spectrum were used to identify the three lines observed in the night sky spectrum as Hg I lines at wavelengths of 4047 Å, 4078 Å, and 4358 Å. The Hg I lines (4047 Å and 4358 Å) are visible on several spectrograms of plates 3a and 3b.

ii) Red Region (4700 - 6000 Å)

The night sky spectrum covering 4700 Å - 6000 Å was photographed at the zenith on the 20 June 1978 using the Varo image tube and a 15 minute exposure (plate I - 010). The spectrum is shown in Figure 10. Using the mercury and sodium lamp spectra, and the OI night sky wavelengths provided by Osterbrook et al. (1976), several of the night sky lines were identified. However, many of the observed features could not be matched with any sodium or mercury wavelengths. No evidence

of sky emission was observed. The locations of the unidentified features along with their approximate wavelengths are shown in Figure 10. Knowing that the reciprocal dispersion changes along the length of an image tube spectrogram (see Chapter 7, page 45), the lack of line identifications in Figure 10, may be possibly attributed to inaccuracies in the listed wavelengths and the resulting poor match when comparing these estimated wavelengths and those of sodium and mercury vapour lamps.

Figure 9

The blue-violet region of the night sky spectrum
observed at the zenith on 24 April 1978 using a class-
ical exposure of 60 minutes. (plate C- 025)

Fig 9, p64

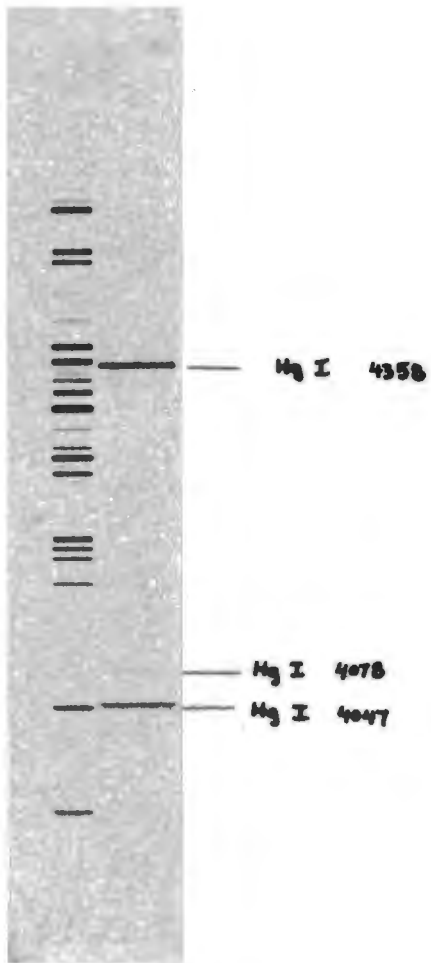
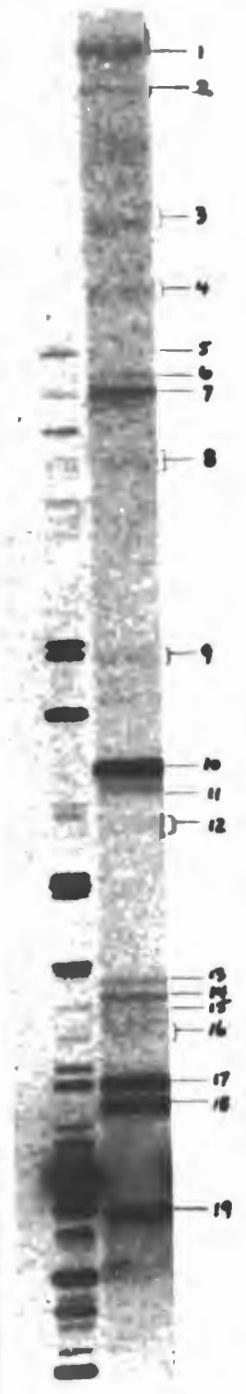


Figure 10

The red region of the night sky spectrum photographed at the zenith on 20 June 1978 using the Varo image tube and a 15 minute exposure. (plate I - 010)



REFERENCE NUMBER.	LINE SOURCE	λ
1	Na I (H. Press. Lamp)	4748
2		~ 4789
3		~ 4910
4	Na I (H. Press. Lamp)	4979, 4983
5		~ 5059
6		~ 5076
7		~ 5090
8	Na I (H. Press. Lamp)	5149, 5153
9		~ 5209
10	Hg I	5461
11		~ 5470
12		~ 5504
13		~ 5663
14	Na I (H. Press. Lamp)	5688, 5688
15		~ 5705
16		~ 5714
17	Hg I	5770
18	Hg I	5791
19	Na I (L. Press. Lamp)	5890, 5896

THESIS RESULTS AND RECOMMENDATIONS

In summary of the results of this thesis, the following facts are noted:-

1. The BGO Atlas provided very good results when classifying unknown program stars. For the 11 stars, the assigned spectral classes were all within 1 subclass of the accepted classifications while 9 out of 11 were assigned the correct luminosity class. In general, all the lines and features used by the Abt-Meinell Atlas for classification were visible on the BGO plates. Pressure broadening of the Balmer lines was observable and provided the primary means of assigning luminosity classes to B and A stars. For the later spectral types, luminosity discriminating lines and ratios were useable.

2. The atlas provided acceptable results when assigning classifications using image tube camera plates. The assigned spectral types were within 3 subclasses and the luminosity classes were correct for 7 of the 11 stars.

3. Two noteworthy items concerning the image tube were the low gain factor observed in the blue-violet region and the distortion of the image tube plate dispersion. The low gain of 5 was explained by a combination of falling tube sensitivity at the shorter blue-violet wavelengths, a slight drop of 0.2 V in the applied d.c. voltage, and the lower sensitivity of the 103a-D emulsion with respect to the 103a -O emulsion which was used for the classical plates. The image

tube dispersion was found to vary with the position on the photocathode ranging from $65 \text{ \AA} / \text{mm}$ about the outer plate edge to $90 \text{ \AA} / \text{mm}$ at the photocathode center.

4. The night sky spectrum in Halifax was examined over the region from 3900 \AA to 6000 \AA . Mercury vapour and sodium (high and low pressure) lamps were found responsible for most of the light pollution.

A review of the major recommendations follows:-

1. To eliminate the difficulties experienced with exposure times, realuminizing of the primary mirror and replacement of the BL 280 grating should be considered.

2. In addition to a new BL 280, a grating blazed at 4000 \AA should be obtained for testing with the image tube system.

3. To ensure a more steady power supply for the image tube, the batteries should be replaced with a controllable power pack.

4. To improve the classification capacity of the BGO Atlas, those gaps noted in Chapter 5 must be filled with suitable MK standards. The atlas must also be strengthened with a sequence of super giant stars

5. A classification atlas for the image tube should also be produced.

APPENDIX A

COMPARISON LINE IDENTIFICATION AND HARTMAN CURVE CONSTRUCTION - CLASSICAL CAMERA

i) Blue - Violet Region ($\lambda < 4600 \text{ \AA}$)

Using the measured line positions (X) obtained from spectrum #12 of focus plate C.T #7, and using the comparison lines #1, 15b, and 20 as the reference points of $\Delta\lambda = 0.0$, the Hartman Dispersion Equation for these lines takes the following forms

$$\text{for line 1, } 4510.73 = \lambda_0 + \frac{C}{30.463 - X_0}$$

$$\text{for line 15b; } 4200.68 = \lambda_0 + \frac{C}{34.145 - X_0}$$

$$\text{for line 20; } 3948.98 = \lambda_0 + \frac{C}{37.145 - X_0}$$

Solving these three equations gives the following solution:-

$$\lambda_0 = - 1.4959526 \times 10^5 \text{ \AA}$$

$$C = 2.814598 \times 10^8 \text{ \AA mm.}$$

$$X_0 = - 1795.941 \text{ m.m.}$$

Using these values, the Hartman equation becomes:-

$$\lambda_m = - 1.4959526 \times 10^5 + \frac{2.814598 \times 10^8}{(X + 1795.941)}$$

Table A.1

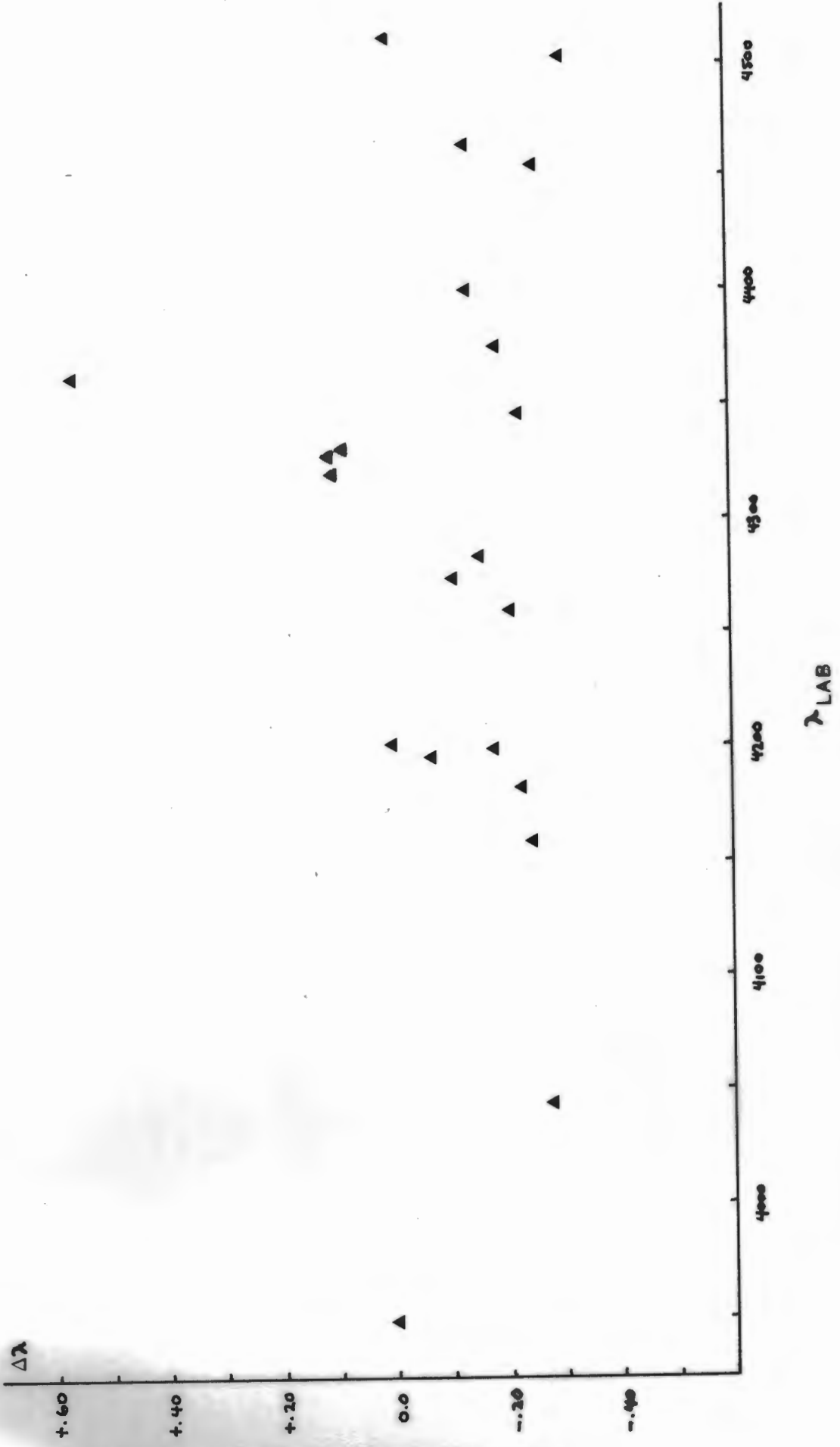
Tabulated below are the measured X values, the calculated Hartman wavelenghts, the comparison line identifications, and the $\Delta\lambda$ values.

Line Reference No.	Source	λ LAB (Å)	TopX(m.m)	Bottom X (mm)	Ave. X	Calc. λ_H	$\Delta\lambda$ ($\lambda_{LAB} - \lambda_H$)
1a	Kr	4502.36	30.563	30.554	30.559	4202.67	-0.31
1b	Ar	4510.73	30.469	30.456	30.463	4510.73	0.0
2	Kr	4463.69	31.023	31.015	31.019	4463.83	-0.14
3	Kr	4453.92	31.139	31.128	31.134	4454.18	-0.26
5	Kr	4399.97	31.780	31.770	31.775	4400.11	-0.14
6	Kr	4376.12	32.063	32.052	32.058	4376.31	-0.19
7	Ne	4363.52	32.220	32.212	32.216	4362.96	+0.56
8	Ar	4345.17	32.430	32.419	32.425	4345.40	-0.23
9a	Ar	4333.56	32.574	32.559	32.567	4333.45	+0.11
9b	Ar	4335.34	32.553	32.537	32.545	4335.26	+0.08
10	Kr	4319.58	32.737	32.726	32.732	4319.48	+0.10
11	Ar	4300.10	32.963	32.949	32.956	4300.67	-0.57
12	Kr	4282.97	33.169	33.160	33.165	4283.13	-0.16
13	Kr	4273.97	33.277	33.267	33.272	4274.08	-0.11
14	Ar	4259.36	33.450	33.439	33.445	4259.57	-0.21
15a	Ar	4198.32	34.175	34.167	34.171	4198.50	-0.18
15b	Ar	4200.68	34.150	34.140	34.145	4200.68	0.0
16	Ar	4191.03	34.265	34.263	34.259	4191.10	-0.07
17	Ar	4181.88	34.372	34.360	34.366	4182.11	-0.23
18	Ar	4158.59	34.649	34.637	34.643	4158.84	-0.25
19	Ar	4044.42	36.008	35.998	36.003	4044.70	-0.28
20	Ar	3948.98	37.152	37.138	37.145	3948.98	0.0

Figure A1

Hartman curve for the blue-violet region (3950 Å - 4525 Å). The curve was constructed from the $\Delta\lambda$ and λ_{Log} values shown in Table A1.

Fig A1, PA3



ii) Red Region ($\lambda > 5000 \text{ \AA}$)

With the measured X values from spectrum 9 of focus test plate C. T #6, and using lines # 3, 19, and 38 as the reference lines of $\Delta\lambda = 0.0$, the Hartman Dispersion Equation for these three lines takes the following forms:-

$$\text{for line 3; } 5400.36 = \lambda_0 + \frac{C}{41.160 - X_0}$$

$$\text{for line 19; } 5944.83 = \lambda_0 + \frac{C}{34.672 - X_0}$$

$$\text{for line 38; } 6506.53 = \lambda_0 + \frac{C}{27.989 - X_0}$$

Solving these three equations gives:-

$$\lambda_0 = -7.1122897 \times 10^5 \text{ \AA}$$

$$C = 6.124292 \times 10^9 \text{ \AA mm.}$$

$$X_0 = -8504.809 \text{ mm.}$$

With these three values, the Hartman equation becomes:-

$$\lambda_H = -7.1122897 \times 10^5 + \frac{6.124292 \times 10^9}{X + 8504.809}$$

Table A2 Data for the Comparison Line Identifications and Hartmann
Curve Construction for the Red Region

Line Reference Number	Source	λ LAB(Å)	Top X (m.m.)	Bottom X	Ave. X	Calculated λ_H	$\Delta\lambda$ ($\lambda_{lab} - \lambda_H$)
3	Ne	5400.36	41.165	41.157	41.161	5400.36	0.0
4	Ne	5562.77	39.227	39.209	39.218	5563.24	-0.47
5	Kr	5570.29	39.132	39.127	39.130	5570.67	-0.62
6			39.007	39.006	39.007	5580.98	
7	Ar	5650.70	38.187	38.178	38.183	5650.12	+0.58
9	Ne	5764.42	36.819	36.811	36.815	5764.89	-0.47
11	Ne	5820.15	36.158	36.154	36.156	5820.22	-0.07
13	Ne	5852.49	35.773	35.765	35.769	5852.71	-0.22
14			35.605	35.597	35.601	5866.81	
15	Kr	5870.92	35.550	35.543	35.547	5871.39	-0.47
16	Ne	5881.90	35.423	35.416	35.420	5882.05	-0.15
17	Ne	5902.46	35.177	35.168	35.173	5902.79	-0.33
19	Ne	5944.83	34.675	34.669	34.672	5944.83	0.0
20	Ne	5965.47	34.429	34.420	34.425	5965.61	-0.14
21	Ne	5975.53	34.311	34.304	34.308	5975.44	+0.09
22	Ne	5987.91	34.162	34.157	34.160	5987.87	+0.04
23			33.870	33.865	33.868	6012.40	
24	Ne	6029.99	33.663	33.654	33.659	6029.95	+0.04
25			33.350	33.344	33.347	6056.12	
26	Ne	6074.34	33.135	33.128	33.132	6074.22	+0.12
27			33.033	33.022	33.028	6082.96	
28	Ne	6096.16	32.877	32.872	32.875	6095.82	+0.34
29	Ne	6128.45	32.490	32.484	32.487	6128.38	+0.07
30	Ne	6143.06	32.321	32.314	32.318	6142.62	+0.44
31	Ne	6163.59	32.078	32.068	32.073	6163.16	+0.43
32	Ne	6217.28	31.437	31.429	31.433	6216.95	+0.33
33	Ne	6266.50	30.850	30.846	30.848	6266.12	+0.38
34	Ne	6304.79	30.395	30.390	30.393	6304.41	+0.38
35	Ne	6334.43	30.041	30.035	30.038	6334.22	+0.21
36	Ne	6382.99	29.464	29.457	29.461	6382.77	+0.22
37	Ne	6402.25	29.235	29.227	29.231	6402.07	+0.18
38	Ne	6506.53	27.992	27.986	27.989	6506.53	0.0
39	Ne	6532.88	27.678	27.676	27.677	6532.77	+0.11

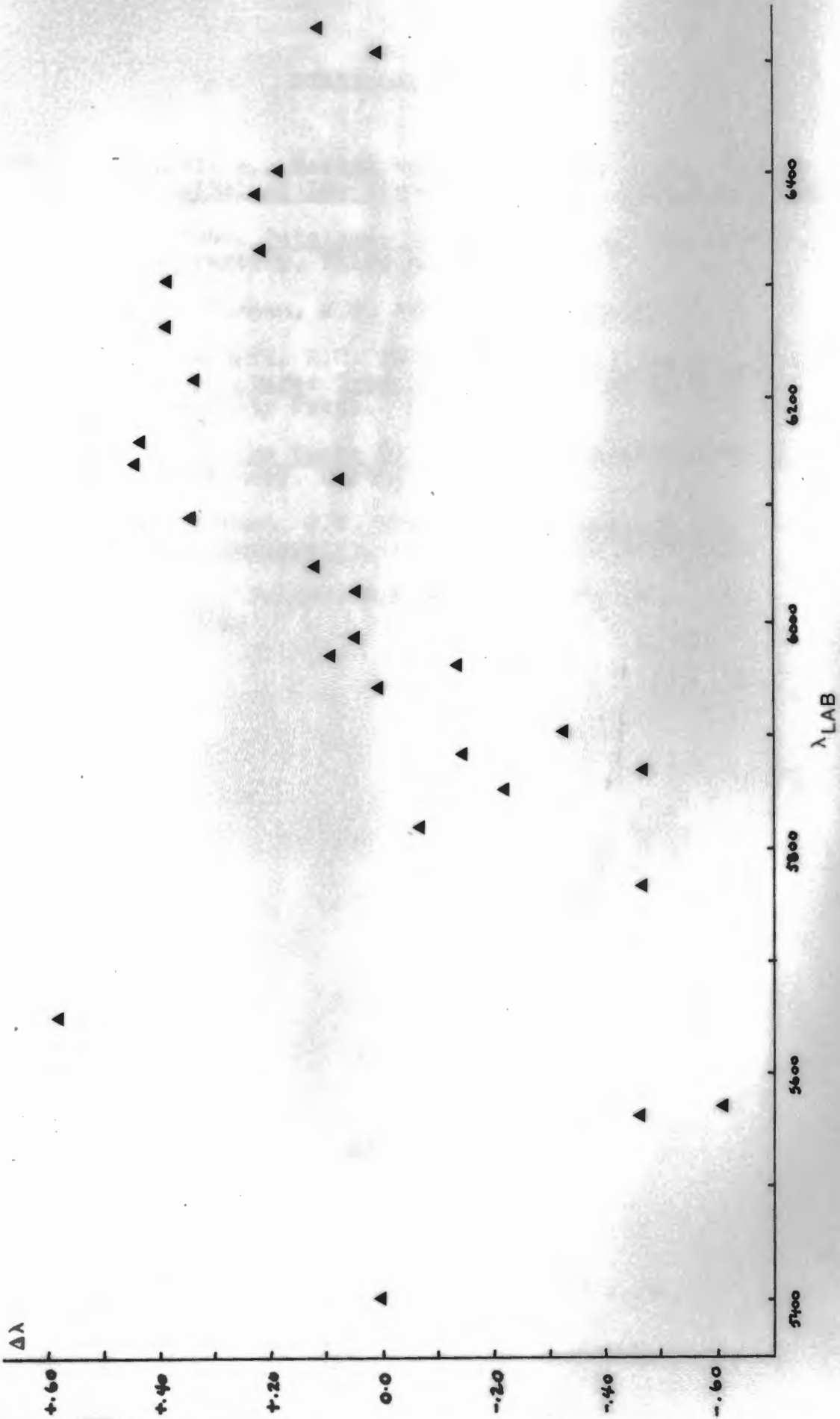
A5

Figure A.2

Hartman curve for the red region (5400 Å - 6525 Å).

The curve was constructed from the $\Delta\lambda$ and λ_{LRS} values listed in Table A.2.

Fig A2, P116



BIBLIOGRAPHY

- Abt, H., Meinel, A., Morgan, W.W., Topscott, J.W., 1968. An Atlas of Low Dispersion Grating Stellar Spectra.
- Hoffleit, D. 1964. Catalogue of Bright Stars, Yale University Observatory, Third Edition.
- Johnson, H.L., Morgan, W.W. 1953. Ap.J. 117,313
- Keenan, P.C., McNeil, R.C. 1976. An Atlas of Spectra of the Cooler Stars: Types G, K, M, S, and C, Ohio State University Press.
- Mook, D.E. 1975, The Spetz Toy Spectrograph at McGraw-Hill Observatory, Dartmouth College.
- Morgan, W.W., Keenan, P.C. 1973. Annual Review of Astronomy and Astrophysics, Vol. 11, ed. L. Goldberg, p. 29.
- Osterbrook, D.E., Walker, M.F., Koski, A.T. 1976., P.A.S.P. 88, 349.